

LIBRARY
ROYAL AIRCRAFT ESTABLISHMENT
BEDFORD.



PROCUREMENT EXECUTIVE MINISTRY OF DEFENCE

AERONAUTICAL RESEARCH COUNCIL

REPORTS AND MEMORANDUM

Pressure Distribution on Two Wings with Curved
Leading Edges at Supersonic Speeds

By K. YEGNA NARAYAN

Cambridge University Engineering Department

LONDON: HER MAJESTY'S STATIONERY OFFICE

1974

PRICE £1.66 NET

Pressure Distribution on Two Wings with Curved Leading Edges at Supersonic Speeds

By K. YEGNA NARAYAN

Cambridge University Engineering Department

*Reports and Memoranda No. 3741**
February, 1973

Summary

Results are presented of a study of the pressures on the flat windward surfaces of two wings with curved, sharp leading edges. The leading edges of one of the wings are convex outwards, whereas those of the second are concave outwards. The wings were tested at nominal free stream Mach numbers of 2.5, 3.5 and 4.5. The results indicate that the changes in flow development due to the curvature of the leading edges are qualitatively similar at all the Mach numbers. In the case of the first wing, the spanwise pressure distribution changed considerably as the flow developed downstream of the vertex. However, the changes in the spanwise pressure distribution on the wing with concave leading edge, though observable, were much less. The pressure distribution on the two wings has been calculated using the concept of an 'equivalent delta wing', but modified to take into account the upstream effect. Comparisons with experiments show that the agreement is fairly good, except at very high incidences and over the outer half of the semi-span. Possible reasons for this discrepancy are discussed. Finally an attempt has been made to justify the definition of an equivalent delta wing based on a simple physical idea.

* Replaces A.R.C. 34 293 and Appendix.

LIST OF CONTENTS

1. Introduction
 2. Apparatus and Tests
 - 2.1. Tunnel
 - 2.2. Models
 - 2.3. Range of test conditions
 - 2.3.1. Cambridge tests
 - 2.3.2. R.A.E. Bedford tests
 - 2.4. Accuracy of the results
 3. Results and Discussions
 - 3.1. Presentation of results
 - 3.2. Discussion of results
 - 3.2.1. Centreline pressure distributions
 - 3.2.2. Spanwise pressure distributions
 4. Prediction of Pressures by an Equivalent Delta-Wing Concept
 5. Discussion of the R.A.E., Bedford Results
 - 5.1. Centreline pressure distributions
 - 5.2. Spanwise pressure distributions
 6. Conclusions
- Acknowledgement
- List of Symbols
- References
- Illustrations—Figs. 1 to 17
- Detachable Abstract Cards

1. Introduction

At the present time, very little is known about the characteristics of wings with curved leading edges in non-linear supersonic or hypersonic flow. A program has therefore been started in the Cambridge University Engineering Department to study the characteristics of such wings at moderately high supersonic Mach numbers. This report presents results from a study of the pressures on two wings of non-conical planform at free-stream Mach numbers of 2.5, 3.5 and 4.5, and at high incidence where non-linear effects are important.

2. Apparatus and Tests

2.1. Tunnel

The investigations were carried out in two different facilities:

(i) the tests at $M_\infty = 2.5$ and 3.5 and at incidences up to about 31 degrees were carried out in the CUED supersonic wind tunnel which is an intermittent blowdown facility and has a working section of 114 mm by 178 mm,

(ii) the tests at $M_\infty = 3.5$ and 4.5 and at incidences greater than 31 degrees were carried out in the 3 ft by 4 ft High Supersonic Speed Tunnel at the Royal Aircraft Establishment, Bedford.*

2.2. Models

Both models have a flat pressure surface and sharp leading edges. Model 'a' has a leading edge which is convex outwards (generally called a Gothic planform) and Model 'b' has a leading edge curved concave outwards (we refer to this as a concave-leading-edge wing). The shapes of the leading edges were chosen so that the shock wave was detached at $M_\infty = 3.51$ and over a range of incidences. This was done by applying the exact two-dimensional oblique-shock relations normal to the leading edge at every point. The planform shapes and the longitudinal and transverse sections of the two models are shown in Fig. 1, which also gives the equations describing the leading edges.

The suction surfaces of both models have a triangular cross-section. It is tacitly assumed however, that the windward side pressures obtained for this particular suction surface shape is representative of other leeward surface shapes also, and in particular of a zero thickness wing. In fact, the experiments of Squire¹ on delta wings have shown that except at very small incidences and close to the leading edges, the suction surface shape has negligible effect on the windward surface pressures.

The models are made out of a high strength alloy steel and for the Cambridge tests were sting mounted on an incidence changing jack which in turn was mounted on the tunnel. For the Bedford tests (since the ratio of the tunnel test-section size to the model size is very large), several models were mounted in the tunnel on a specially designed model carrying system (Fig. 11 shows the model carrier). The models (including some from other studies) were mounted one above the other in the vertical plane, the spacing between the models being decided by two factors, (a) minimum interference between the models, and (b) maximum allowable overall length of the model carrier. The model carrier was mounted on the sting carrier shaft which in turn was mounted on a moving quadrant. The sting carrier shaft could be controlled in pitch through a total range of 32 degrees (5 degrees depression and 27 degrees elevation) with respect to the horizontal. The models themselves were individually mounted on the carrier at various angles (Fig. 11) with respect to the horizontal to get a higher range of incidence.

To measure the static pressures, a number of hypodermic tubes of 1.626 mm OD and 1.092 mm ID were laid in suitably milled grooves running in the streamwise direction. The grooves were then filled with Araldite and the surface hand polished to get as smooth a surface as possible. At any one time, the pressures at one chordwise station only could be measured. After these pressures had been measured, the set of static holes were sealed with paraffin wax and holes at the subsequent chordwise position were then drilled. All the static pressure holes had a diameter of 0.3046 mm.

2.3. Range of Test Conditions

2.3.1. Cambridge tests. The tests were made at nominal free stream Mach numbers of 3.51 and 2.49 respectively. The corresponding free stream Reynolds numbers are 51×10^6 per metre and 30.3×10^6 per metre.

* The author thanks Dr. L. Pennelegion, R.A.E., Bedford for granting permission to use the tunnel and Mr. G. V. F. Smith for his assistance in planning and conducting the experiments at Bedford.

The angle of incidence (defined with respect to the plane of the leading edge, which in these cases is the same as that of the pressure surface) was varied in 4 degree steps for the Gothic wing and in 2 degree steps for the concave-leading-edge wing. The maximum angles of incidence ($31^{\circ} 35'$ and $27^{\circ} 20'$ for the Gothic wing at $M_{\infty} = 3.51$ and 2.49 respectively, $26^{\circ} 51'$ and $22^{\circ} 54'$ for the concave-leading-edge wing at the two Mach numbers) were governed by considerations of flow breakdown in the tunnel. In fact, even at these values of the incidences the boundary layer on the floor of the test section separated due to the strong shock wave of the wing. However, as judged from the schlieren photographs, the reflected wave system passed sufficiently far downstream of the region of interest so as not to produce any noticeable changes in the flow field of the wing.

The pressures were measured on a conventional multitube mercury manometer referred to atmospheric pressure.

Schlieren and shadowgraph studies were made for both the models at the two Mach numbers. The schlieren system in these tests was a conventional two-mirror horizontal Z-shape light-path system used with vertical cut off. All the runs were made with natural transition of the boundary layer.

2.3.2. R.A.E., Bedford Tests. These tests were made at Mach numbers of 3.5 and 4.5. The corresponding free stream Reynolds numbers were 22.6×10^6 per metre and 27.2×10^6 per metre. The angle of attack was varied in steps of about 5 degrees from 32 to 62 degrees (concave-leading-edge wing) and from 32 to 61 degrees (Gothic wing).

Since the number of tunnel runs was limited, only a limited number of static pressure holes were used. The pressure distributions obtained in the Cambridge tests were used as a guide in the selection of the static pressure holes to give maximum coverage of data. The pressures were sensed by a transducer and recorded. The scanning operation was controlled manually and sufficient time was given (about 2 minutes) before the data was logged and scanning continued. Once all the ports had been scanned, the angle of attack was changed and the process repeated.

These tests were also made with natural transition of the boundary layer.

2.4. Accuracy of the Results

Experimental inaccuracies arise from such sources as non-uniformity of the flow in the test section, inaccuracies in the manometer, lags in the pressure tubes and errors due to imperfections at the static pressure holes.

Over the region occupied by the model, non-uniformities in the test section flow account for variations in Mach numbers of ± 0.04 in the 3.5 liner and of ± 0.05 in the 2.5 liner. The variations in the flow directions are about ± 0.2 degrees in the 3.5 liner and ± 0.3 degrees in the 2.5 liner. These correspond to errors in C_p of ± 2 percent in the 3.5 liner and ± 4 percent in the 2.5 liner.

The pressure can be read in the manometer to an accuracy of ± 0.05 mm of Hg. A similar figure applies to the reference pressure also. Therefore, the pressure is accurate to ± 1 mm of Hg. At both nominal free stream Mach numbers of 3.51 and 2.49, this corresponds to an error in C_p of ± 0.002 .

It is thought that errors due to lags in the pressure lines are negligible since the pressure levels were quite high and sufficient time was given for the pressures to settle down before the manometer was frozen. Furthermore, results with increasing and decreasing incidence showed hardly any noticeable difference.

The angle of incidence was found to be repeatable to within ± 10 minutes. Previous experience with the incidence changing jack (Hillier²) has shown that during a run, the aerodynamic loads on the model did not cause any noticeable deflection of the model. Thus the angles of incidence quoted in the figures are subject to inaccuracies of about ± 10 minutes.

The errors involved in the R.A.E., Bedford tests are expected to be smaller than the values quoted for the Cambridge tests.

Another error which needs to be considered is that due to the lateral asymmetry of the model. Static pressure holes are provided on either side of, and staggered off the centreline, mainly to obtain a fuller coverage across the span. This incidentally helps in assessing the errors due to lateral asymmetry of the model. For example, the wiggles perceptible in many of the spanwise pressure distributions can in part be attributed to such an asymmetry. An examination of the pressure distributions indicate that a majority of the results lie within a scatter band about ± 0.015 in C_p .

Viscous effects are not thought to be of much importance since the non-linear effects typical of a hypersonic environment have been produced at relatively moderate Mach numbers by having high angles of incidence. Furthermore, the fact that the Reynolds numbers are high would also suggest that viscous interaction effects are not likely to have any noticeable effect on the flow field.

3. Results and Discussions

3.1. Presentation of Results

Static pressures were measured on either side of the model centreline and at various chordwise positions. The spanwise coordinate is non-dimensionalised by the local semi-span b . All pressures are presented in the form of the pressure coefficient C_p .

Centreline pressure distributions for the two wings at all Mach numbers and over the full range of incidence are given in Figs. 2a through 2d (Cambridge tests) and 13a through 13d (Bedford tests). The spanwise pressure distributions are shown in Figs. 3 through 6 (Cambridge tests) and Figs. 14 through 17 (Bedford tests). A majority of the experiments has been repeated more than once and the data shown in the figures are the mean of the runs. In no case however, was the difference in C_p between any two runs greater than the uncertainty quoted in Section 2.4.

Since the measurements have been made in two different facilities, it is necessary to check that the two sets of results are consistent. The obvious way of doing this is to plot the pressures at selected points as functions of angle of attack. Typical results are presented in Fig. 12. From the figure it is clear that the two sets of results are fully self-consistent. It is of particular interest to note that the two centreline data merge smoothly with the Cole and Brainerd³ solution for the slender wings at angles of attack near 90 degrees.

3.2. Discussion of Results

Since frequent reference will be made to the thin-shock-layer theory, we begin the discussion with a very brief outline of the theory itself.

The theory of thin shock layers, as developed by Messiter⁴ for slender delta wings of zero thickness (and later extended by Hida,⁵ Squire⁶ to include thickness effects) consists of expanding the flow variables in terms of a density ratio ε across the shock wave assumed to lie in the plane of the leading edges.

$$\left(\text{Here } \varepsilon = \frac{\gamma - 1}{\gamma + 1} + \frac{2}{(\gamma + 1)M_\infty^2 \sin^2 \alpha} \right).$$

The equations of motion and the boundary conditions are then simplified on the assumption that ε is small and terms involving second and higher powers of ε can be neglected. The zeroth order solution ($\varepsilon = 0$) corresponds to the simple Newtonian result. To the first order in ε , it can be shown that the flow field depends on two similarity parameters Ω and C which are the sweep back and the thickness of the wing in a transformed plane. In fact, $\Omega = \cot \Lambda / \varepsilon^{1/2} \tan \alpha$ and $C = h / \varepsilon^{1/2} \cot \Lambda$ where Λ is the sweep back angle, h is the thickness of the wing and α is the incidence, the last two being measured with respect to the plane of the leading edge. Detailed discussions of the theory are available in Ref. 2; we will not therefore discuss it here again, but simply point out that the shock stand-off distance y_s (measured normal to the wing surface) and C_p at any spanwise position z/b on a conical wing can be written as

$$\frac{y_s}{x}(z/b; \Omega, C) = \varepsilon \tan \alpha y^*(z/b; C, \Omega)$$

and

$$C_p(z/b; \Omega, C) = 2 \sin^2 \alpha (1 + \varepsilon p^*(z/b; \Omega, C) + 2C\Omega\varepsilon),$$

where y^* and p^* are functions which are obtained as solutions of the simplified equations of motion. Squire⁷ has given detailed charts of y^* and p^* as functions of C with Ω as a parameter and for different values of the spanwise co-ordinate z/b . All the calculations made in this report are based on these charts. It has been shown by Squire⁷ that the error in C_p calculated using these charts is $\mp 0.01 (\sin^2 \alpha + 5/M_\infty^2)$ for $\gamma = 1.4$.

In what follows, the Cambridge tests are discussed fully at first, as is the concept of the 'equivalent delta wing' suggested for the prediction of pressures. The information gained in these sections is then used to interpret the data obtained from the Bedford tests (Section 5).

3.2.1. Centerline Pressure Distribution. Figures 2 (a through d) show the centreline pressure distributions. Figures 2a and 2b refer to the Models a and b respectively at $M_\infty = 3.5$ while 2c and 2d refer to $M_\infty = 2.5$. For practical reasons, pressures could not be measured upstream of $x/c = 0.2$ and $x/c = 0.4$ in the two models respectively. However, the range of x/c covered is wide enough to establish certain general trends. The chain dashed line in each figure represents the C_p corresponding to a conical wing of sweep back angle equal to that of the given wing at the vertex,* calculated using thin shock layer theory (Squire⁷).

* We refer to this in future as vertex conical flow for brevity.

It is seen from Figs. 2a and 2b that while the pressures decrease from the vertex downstream in Model 'a', they remain more or less constant in Model 'b'. An interesting feature of the results is that the pressures on the Gothic wing upstream of $x/c \simeq 0.3$ agree quite well with C_p corresponding to the vertex conical flow. (The agreement at lower incidences (typically $\alpha \lesssim 13$ degrees) is not so good, but this presumably is due to the doubtful validity of the thin shock theory itself at large values of ε .) Furthermore, the pressures on the concave leading edge wing at all x/c (again at the higher incidences) agree rather well with the theoretical value of C_p corresponding to the vertex conical flow.

Results from the $M_\infty = 2.5$ measurements (Figs. 2c and 2d) indicate that the pressures generally decrease downstream of approximately $x/c = 0.3$ in the Gothic wing and increase downstream of the same station in the concave-leading-edge wing. Furthermore, the pressures on both the wings upstream of $x/c = 0.3$ seem to approach the theoretical pressure corresponding to the respective vertex conical flows.

The behaviours mentioned above can be explained by referring to Fig. 8, which is a plot of the function p^* at $z/b = 0$ versus the parameter Ω (Ω is the only parameter to be considered since we are considering flat wings). Now, at each point of the leading edge of the wings under consideration, we can define a local sweepback angle and thus a corresponding Ω_{LOCAL} . Indicated in the figure are the values of Ω at the vertex (Ω_v) and the Ω_{LOCAL} at $x/c = 1$, for the two models at both Mach numbers and at the maximum and minimum values of the incidence.

Considering the $M_\infty = 3.5$ results first, it is clear that at all incidences, the Gothic wing lies in a region where p^* depends rather strongly on Ω . The concave-leading-edge wing on the other hand lies much further to the right in the plot, in a region where p^* is only a relatively weak function of Ω . Furthermore the variation of Ω from the vertex to the trailing edge in the Gothic wing is more by a factor of about three than the corresponding variation in the concave-leading-edge wing. Therefore, the experimental data show a large change in the pressures downstream of the vertex in the Gothic wing, whereas in the concave-leading-edge wing, it is more or less constant.

Similar arguments apply to the $M_\infty = 2.5$ results: the concave-leading-edge wing is shifted to the left in Fig. 8 and thus the pressures do show a noticeable change downstream of the vertex.

These results seem to suggest that we can discuss qualitatively the general behaviour of a wing with curved leading edges based on the local values of Ω . However, as will be discussed later, the changes are always over-estimated by using Ω_{LOCAL} .

3.2.2. Spanwise Pressure Distributions

Model 'a': Figs. 3 and 4 show the pressure distributions in terms of C_p versus z/b at Mach numbers 3.5 and 2.5 respectively. The chain-dashed lines in each figure represent the theoretical C_p distribution corresponding to the vertex conical flow, calculated using the thin-shock-layer theory. It is seen from the figures that the pressure distribution changes appreciably as the flow develops downstream of the vertex. At $M_\infty = 3.5$ and $x/c = 0.2$ and 0.3 , the results seem to be in reasonable agreement with the calculated vertex conical flow over the central 50 per cent of the span. (Due to practical reasons, results could not be obtained closer to the leading edge.) It should be noted that even in this region, the flow is not conical, but rather the pressures are constant along lines $z/b = \text{constant}$. The distributions from $x/c = 0.2$ to $x/c = 0.5$ show that the pressures are lowest near the centreline and increase outboard, which of course is characteristic of flat wings of moderate and large aspect ratios. This, as has been pointed out by Squire,¹ is because the flow about a flat wing of large aspect ratio in sections parallel to the free stream, tends to be similar to the flow past a flat plate with a detached shock wave: thus the pressure is highest at the leading edge and falls off inboard. The magnitude of the increase in C_p from the centreline outboard however decreases with x/c . (This of course is due to the decreasing local Ω .) At $x/c = 0.6$, the pressures at higher incidences are almost uniform across the span up to about $z/b = 0.7$, which is the last measurement station. At lower incidences (typically $\lesssim 13^\circ$), the pressures increase very slightly outboard. Downstream of $x/c = 0.6$, the pressure decreases from the centreline outboard, which is characteristic of the flow over an inclined cone (or equivalently a thick wing). This suggests, again following Squire,¹ that the flow about a flat wing of small aspect ratio is three-dimensional and the high pressure at the centre is associated with a normal cross-flow shock there.

The same comments apply to the $M_\infty = 2.5$ results; the cone flow behaviour is particularly pronounced here, as can be seen from the pressure distributions at $x/c = 0.7, 0.8$ and 0.9 .

Model 'b': Figs. 5 and 6 show the corresponding pressure distributions. The most interesting feature of the $M_\infty = 3.5$ pressure distributions is the fact that right up to $x/c = 0.9$, the distribution over the central 40 per cent of the wing span shows hardly any noticeable change compared with the vertex conical flow. Outboard of $z/b \simeq 0.5$, the measured pressures are higher than the pressures at corresponding points in a delta wing of sweep back angle the same as that of the given wing at the vertex. This is not surprising since arguments

based on the local sweep back angle also suggest the same. However, as was mentioned earlier, the changes in the pressure distribution are overestimated by a purely local calculation.

In the case of the $M_\infty = 2.5$ results, the centreline pressure, as discussed in Section 3.2.1, increased downstream of the vertex. Therefore, except at $x/c = 0.4$, the pressure distributions show noticeable differences from the vertex conical-flow results. Some of the low incidence results (for *e.g.* $\alpha = 13^\circ 46'$ at $x/c = 0.4$ through 0.9) show a remarkable agreement with the corresponding vertex conical-flow results. This agreement could be completely fortuitous since the 'small' parameter ε of the thin-shock-layer theory is more than 2 and the validity of the approximation needs careful assessment.

4. Prediction of Pressures by an Equivalent Delta-Wing Concept

It was mentioned in the earlier sections that we can define at every point of the leading edge of the wing a local sweep-back angle and thus a local value of the parameter Ω . Further, we have also seen that the behaviour of the wing can be qualitatively explained by considering the local Ω (Ω_L) in conjunction with thin-shock-layer theory. It would seem appropriate that we enquire whether the pressures calculated based on Ω_L agree with the experiments. (This approach can be termed as a 'local conical' approximation.) Calculations were thus made of the spanwise pressure distributions for the two wings at both Mach numbers and over the full range of incidence. The results are shown in Figs. 2 through 6 as dashed lines. From Figs. 2 (a to d), it is clear that the trend is predicted correctly though the magnitudes of the pressure are not correct. The same conclusion can be drawn from the spanwise pressure distributions also (Figs. 3 through 6). The experimental data in all the cases lie between the vertex conical and the local conical flow results. Furthermore it seems that the difference between the experimental data and the local conical flow result decreases as one moves outboard from the centreline of the wing. This fact is not surprising since one would expect the flow at the leading edge to be dominated by local conditions.

From the preceding discussion, it is clear that the flow at any point on the wing is influenced by both local conditions and conditions upstream of it, the local condition having a larger influence closer to the leading edge. In calculating the pressure distribution therefore, one would have to allow for this upstream effect, which itself varies across the span. One of the simplest methods of doing this is to define an 'equivalent' delta wing at each spanwise station. The 'equivalent' delta wing, characterised by the parameter Ω_e , is expressed as a function of the vertex conical wing (which is assumed to characterise the upstream effect) and the local conical wing (to account for the local effect), say of the form

$$\Omega_e(z/b, x/c) = a_1\Omega_v + a_2\Omega_L(x/c)$$

a_1 and a_2 are necessarily functions of z/b . It is neither obvious nor possible to determine a_1 and a_2 precisely; the best possible values can only be found by trial and error. It was found that the values $a_1 = (2 - z/b)/4$ and $a_2 = (2 + z/b)/4$ gave reasonably good agreement with the experiments. Thus, the pressure at any point of the given wing is that at a corresponding point on an 'equivalent' delta wing defined by $\Omega_e(z/b, x/c) = (2 - z/b)/4\Omega_v + (2 + z/b)/4\Omega_L(x/c)$. On the centreline ($z/b = 0$), the influence of the vertex and the local flows are equal. Note that at the leading edge, the equivalent delta wing is not the local delta wing as one would expect.

The solid lines in all the figures (2 through 6) represent the pressures calculated using this equivalent delta wing definition from the charts presented by Squire⁷ for conical wings. As can be judged from the figures, the agreement between the prediction and experiments is in general very good. However, since there are not many experimental data outboard of $z/b \simeq 0.8$, it is very difficult to argue on the accuracy of the method closer to the leading edge. But judging from the results of the concave-leading-edge wing, where there are some experimental data up to $z/b = 0.9$, we suggest that the method gives reasonable results at least up to $z/b = 0.9$. In passing, it should be noted that even for conical wings, the accuracy of the thin-shock-layer calculations close to the leading edge is not established.

Using the same definition of Ω_e , the shock shape y_s can also be calculated from the charts of y^* presented by Squire.⁷ Figs. 7a and 7b show the centreline shock stand-off distance plotted as a function of the streamwise distance x for the two wings at both Mach numbers and at typical values of angles of incidence. It is seen from the figures that the shock is curved, although the curvature is only just noticeable. In the Gothic wing, the shock moves inwards (towards the body) with the streamwise distance, whereas in the concave-leading-edge wing, it moves outwards from the body. There are reflected in the corresponding pressure distributions (pressures decreasing downstream of the vertex in the Gothic wing and increasing in the concave-leading-edge wing).

Also shown in the figures (by circles) is the centreline shock stand-off distance measured from the shadow-graph pictures of the flow field. The agreement between the estimation and the measurement appears to be

reasonably good, although in some cases ($M_\infty = 3.5$, $\alpha = 17^\circ 58'$ and $M_\infty = 2.5$, $\alpha = 16^\circ 7'$ concave-leading-edge wing; $M_\infty = 3.5$, $\alpha = 31^\circ 35'$ Gothic wing), the shock curvature seems to be slightly overestimated by the calculation. The disagreement in the $M_\infty = 3.5$, $\alpha = 17^\circ 58'$ (concave-leading-edge wing) and $M_\infty = 3.5$, $\alpha = 31^\circ 35'$ (Gothic wing) is however within the uncertainty in measuring the shock stand-off distance. The disparity in the case of $M_\infty = 2.5$, $\alpha = 16^\circ 7'$ (concave-leading-edge wing) is relatively much larger.

A plausible explanation for the success of the prediction method discussed in the preceding paragraphs can be given as follows. Let us consider two points A and B on the surface of, say, the Gothic wing—one (A) on the centreline and the other (B) closer to the leading edge. The domains of dependence of these points are the regions bounded by the fore Mach cones from the points. The Mach lines can be drawn if we know the Mach number distribution in the shock layer. The Mach number distribution is calculated using the measured pressure distribution and the shock shapes calculated using the 'equivalent' delta wing concept. Fig. 9 shows the Mach lines from the points A and B at $M_\infty = 3.5$ and at two incidences $13^\circ 29'$ and $31^\circ 35'$ (lines AA_1 and AA_2 respectively). (Note that the curvature of the Mach lines due to the non-uniform Mach number distribution in the shock layer has been neglected.) The 'equivalent' delta wing appropriate to the point A is therefore the one corresponding to A_1 or A_2 , depending on the incidence. At any one incidence, however, the difference in Ω between A_1 and A_2 is quite small: the same 'equivalent' delta wing is therefore used at all incidences. Furthermore A_1 and A_2 both lie roughly halfway between 0 and A' (the vertex and $x/c = 0.5$). Thus the use of an Ω_e which is the mean of Ω_v and Ω_l seems to be reasonable.

Also shown in the figure is the domain of dependence of a point B which is at 70 per cent semispan from the centreline. It is seen that the Mach lines BB_1 and BB_2 intersect the leading edge closer to A' than AA_1 and AA_2 , confirming that the local influence is in fact stronger than the influence from the vertex. Furthermore, here also, the difference in Mach angles between the highest and lowest incidence is quite small. Thus the sort of the 'equivalent' delta wing suggested seems to be reasonable over the full incidence range.

Similar arguments apply for other points on the wing, as well as at $M_\infty = 2.5$.

In Fig. 10 is plotted the Mach angle μ_2 in the shock layer ($x/c = 0.5$ for the Gothic wing) as a function of the incidence α for various Mach numbers. Also shown are the $\epsilon = 1$ line and the line to the left of which the shock is attached near the vertex. The maximum μ_2 ($\alpha = 27^\circ$ at $M_\infty = 2.5$) and the minimum μ_2 ($\alpha = 14^\circ$ at $M_\infty = 3.5$) obtained from the experimental data are also marked in the figure. Thus, it would appear that within this range of μ_2 , the suggested definition of an 'equivalent' delta wing gives reasonable results.

5. Discussion of the R.A.E., Bedford Results

5.1. Centreline Pressure Distributions

Since only a limited number of runs were made, a full coverage in x/c could not be obtained. The points which are shown flagged have been obtained by interpolation of the corresponding spanwise pressure distributions. Also shown in the figures are the pressure distributions for the vertex conical flow (chain-dashed line) and the pressures for the local conical flow (dash-dot line).

Considering the concave-leading-edge wing first (Model b, Figs. 13a and 13b), at both Mach numbers and at all angles of attack, there is a tendency for the pressures to increase slightly; furthermore, the pressures seem to follow the trend suggested by the local conical theory. It should be noted, however, that the difference between the local and the vertex flow results is small. For example, the calculated local C_p is just 3 per cent greater than the calculated vertex C_p .

For the Gothic wing (Model a, Figs. 13c and 13d), the pressures decrease downstream from the vertex. The differences between the local flow and the vertex flow pressures are considerable and the experimental data fall roughly between them at the lower end of the incidence range. At the higher incidences, there is an indication that the pressures tend to follow the local flow result more closely.

Looking at the trend of the pressure variations, it appears that the sort of approximation given earlier for low incidences [$\Omega_e = (\Omega_v + \Omega_l)/2$] is good up to incidences of about 40 to 45 degrees. Beyond this, a better approximation would seem to be to consider the local flow itself. This behaviour is to be expected for the following reason. At low angles of attack (say < 30 to 35 degrees) and at moderately high Mach numbers (> 2.5 to 3), the Mach number in the shock layer is still reasonably high. The fore Mach cone from any point on the wing is thus swept considerably forward (see Fig. 9). Therefore, the point under consideration is likely to be influenced considerably by a region close to the vertex and hence some averaging of the vertex and local flows gives the right pressure. As the angle of attack increases, the Mach number in the shock layer decreases, thus the Mach lines from any point on the wing will be swept much less forward than at lower incidences. This implies that the region of influence of the point is much larger and includes portions of the leading edge much closer to the point. On general grounds, one might expect that even within the region of influence, the

regions closer to the point have a larger influence on it than the regions far from it. Therefore, at high incidences the pressures should follow the local flow results more closely.

At the two highest incidences for $x/c > 0.8$, the pressures on both wings show marked departures from earlier behaviour. This is thought to be due to the interference between the models.

5.2. Spanwise Pressure Distributions

These are shown in Figs. 14 and 15 for Model b at $M = 3.5$ and 4.5 respectively and in Figs. 16 and 17 for Model a at the two Mach numbers. Also plotted in the figures are the results for the vertex conical flow (chain dashed line) and the local conical flow (dash-dot line), both calculated using thin-shock-layer theory.

Considering the concave-leading-edge wing (Model b) first, at both Mach numbers and at all chordwise stations, the pressure distributions at the low incidences show an outward positive pressure gradient, characteristic of moderate and large aspect ratio wings. Furthermore, the increase in pressure outboard seems to be increasing slightly with x/c , this of course is to be expected because the sweepback decreases with x/c . As the incidence is increased, the pressure distribution becomes uniform and then starts to exhibit the outward negative pressure gradient, characteristic of a small-aspect-ratio wing. Once the pressure distribution has changed from one of outward increasing type to one of outward decreasing type, the outward negative gradient increases with angle of attack at all chordwise stations.

The differences between the calculated vertex C_p and the calculated local C_p are small, again being just greater than the experimental uncertainties. The pressures are predicted well by the local flow calculations (or by the vertex flow for the reason mentioned above) up to about 40 degrees incidence. Beyond this, the experimental pressures outboard of 50 to 60 per cent semi-span decrease much more rapidly than the calculations show, although inboard of 50 to 60 per cent semi-span, the pressures are given well by the local flow calculations. It is interesting that the incidence range over which the character of the pressure distribution changes from one of outward positive gradient to one of negative gradient is reproduced quite faithfully by the local flow calculations.

The Gothic wing pressure distributions downstream of $x/c = 0.4$ all belong to the outward negative gradient type. In this case, the difference between the local flow and the vertex flow is much larger. At the lower end of the incidence range the experimental data fall between the vertex and the local flow results, an approximation of the kind suggested earlier for low incidences (i.e. $\Omega_e = (2 - z/b)/4\Omega_v + (2 + z/b)/4\Omega_L$) may thus be expected to give the right pressures. As the angle of attack increases, however, the experimental data are seen to be in better agreement with the local flow results (presumably for the reason already discussed) over the inboard 50 to 60 per cent of the wing semi-span. Outboard of this, the pressures decrease much more rapidly than either the local flow or the low incidence approximation would seem to indicate.

Summarising, we might say that the concept of an 'equivalent' delta wing is useful in predicting the form and magnitude of the pressure distribution on wings of non-conical planform. The approximate definition of an 'equivalent' delta wing

$$\Omega_e(x/c, z/b) = \frac{2 - z/b}{4} \Omega_v + \frac{2 + z/b}{4} \Omega_L(x/c)$$

holds as long as the average Mach number in the shock layer is around 2; this means that the Mach angle in the shock layer is around 30 degrees. At very high incidences (which from the experimental results seems to be > 40 degrees), the pressures seem to be well predicted by a purely local calculation, inboard of about 60 per cent semi-span. Note that at very high free stream Mach numbers, ϵ is very small so that the perturbation ϵp^* on the Newtonian flow is also very small. The difference between the vertex and the local flow is thus small, and for a first approximation, either result may be considered.

Possible reasons for the rapid decrease of pressure outboard of 60 per cent semi-span at high angles of attack are now discussed. As the angle of attack increases, the magnitude of the chordwise component of the velocity decreases (roughly like $\cos \alpha$), while the spanwise component increases. In fact, at the Cole and Brainerd limit (slender wing at near 90 degrees to free stream), the only velocity that needs to be considered is the spanwise velocity. Spanwise strip theory is thus valid and the results immediately show that the centreline is a stagnation line and the leading edge a sonic line. In this model, the pressure distribution would show a rapid decrease of pressure from the stagnation value on the centreline to the sonic value at leading edge.

Another and probably a stronger reason (particularly since the phenomenon has been noted at much lower incidences than is normally considered (> 75 degrees) for the validity of the Cole and Brainerd theory), could be the upper surface effect. All the calculations have been made with the assumption that the upper surface has no effect on the lower surface flow. This is valid at moderate angles of attack when the upper surface flow

is attached at the leading edge with supersonic expansion around the leading edge. At higher angle of attack, the upper surface flow is of the fully separated type,⁸ thus invalidating the important assumption of independence of upper and lower surfaces. In particular, the lower pressure on the upper surface can communicate to the lower surface. This would then induce a larger increased spanwise outflow than the theory indicates on the lower surface, thus accounting for an increased shock curvature and a decreasing pressure towards the leading edge. What is not clear at this stage, however, is the range of angles of attack over which the upper surface flow becomes fully separated and the extent of the interaction between the two surfaces. This problem needs further investigation, possibly with the simpler ordinary delta wing.

6. Conclusions

Centreline and spanwise pressure distributions on two flat wings of non-conical planforms are given at three supersonic Mach numbers. The changes in the flow due to the curved leading edge as compared to a wing with straight leading edges have been explained qualitatively based on local values of Ω . Quantitatively, it has been possible to predict the pressures on the two wings at all the Mach numbers and over a certain range of incidence based on the 'equivalent delta wing' concept. An attempt has been made to justify the success of the concept and possible situations where it might fail are also indicated.

Acknowledgement

The author would like to express his sense of gratitude to his research supervisor, Dr. L. C. Squire for suggesting this problem and for his continued help and guidance throughout the course of this work. He would also like to thank the authorities of Churchill College for the award of a Pochobradsky Research Studentship.

LIST OF SYMBOLS

C_p	Pressure Coefficient = $\frac{p - p_\infty}{\frac{1}{2}\gamma p_\infty M_\infty^2}$
M_∞	Free stream Mach number
p_∞	Free stream static pressure
p	Static pressure at any point
b	Local semi-span
c	Root chord
a_1, a_2	Functions of z/b in the definition of the 'equivalent' delta wing
x, y, z	Cartesian co-ordinate system
α	Angle of incidence w.r.t. plane of the leading edges
γ	Ratio of specific heats
ε	Inverse of density ratio across shock wave lying in the plane of the leading edges
	$= \frac{\gamma - 1}{\gamma + 1} + \frac{2}{(\gamma + 1)M_\infty^2 \sin^2 \alpha}$
Λ	Sweepback angle of leading edge
Ω	Reduced aspect ratio = $\frac{\cot \Lambda}{\varepsilon^{\frac{1}{2}} \tan \alpha}$

REFERENCES

- | <i>No.</i> | <i>Author(s)</i> | <i>Title, etc.</i> |
|------------|------------------------------------|--|
| 1 | L. C. Squire | Pressure distributions and flow patterns at $M = 4.0$ on some delta wings.
A.R.C. R. & M. 3373 (1963). |
| 2 | R. Hillier | Some applications of thin shock layer theory to hypersonic wings.
Ph.D. Thesis, Department of Engineering, Cambridge University.
(1970). |
| 3 | J. D. Cole and J. J. Brainerd .. | Slender wings at high angles of attack in hypersonic flows.
<i>Hypersonic Flow Research</i> (Ed. F. R. Riddell), p. 321, Academic Press, New York (1962). |
| 4 | A. F. Messiter | Lift of slender delta wings according to Newtonian theory.
<i>AIAA Journal</i> , Vol. 1, p. 794 (1963). |
| 5 | K. Hida | Thickness effects on the force of slender delta wings in hypersonic flow.
<i>AIAA Journal</i> , Vol. 3, p. 427 (1965). |
| 6 | L. C. Squire | Calculated pressure distributions and shock shapes on thick conical wings at high supersonic speeds.
<i>Aero. Quart.</i> , Vol. XVIII, p. 185 (1967). |
| 7 | L. C. Squire | Calculations of the pressure distributions on lifting conical wings with applications to the off-design behaviour of wave-riders.
<i>AGARD Conf. Proc.</i> , No. 30 (1968). |
| 8 | J. P. Reding and L. E. Ericsson .. | Review of delta-wing space shuttle vehicle dynamics.
NASA TM X-2508, p. 861 (1972). |

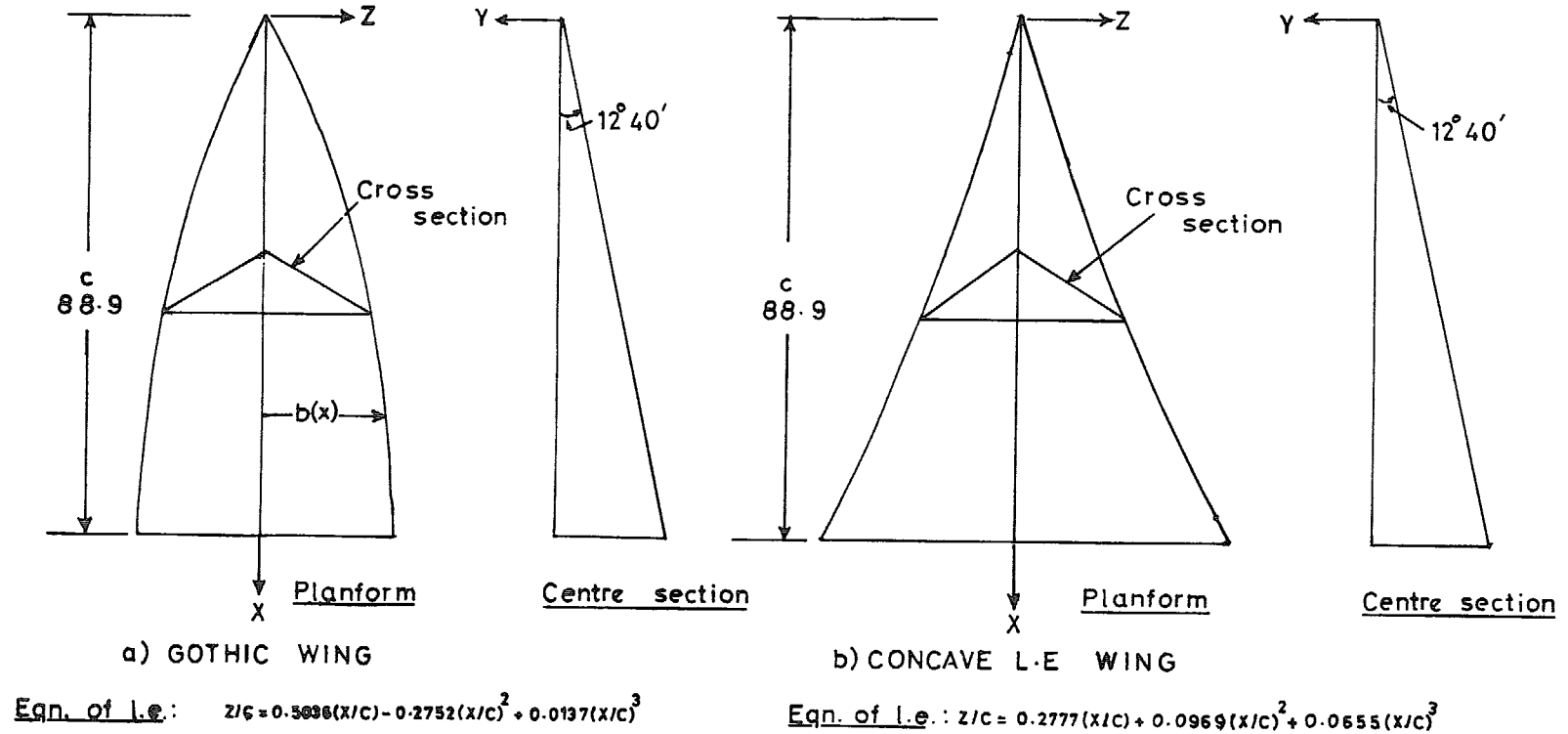


FIG. 1. Details of wings.

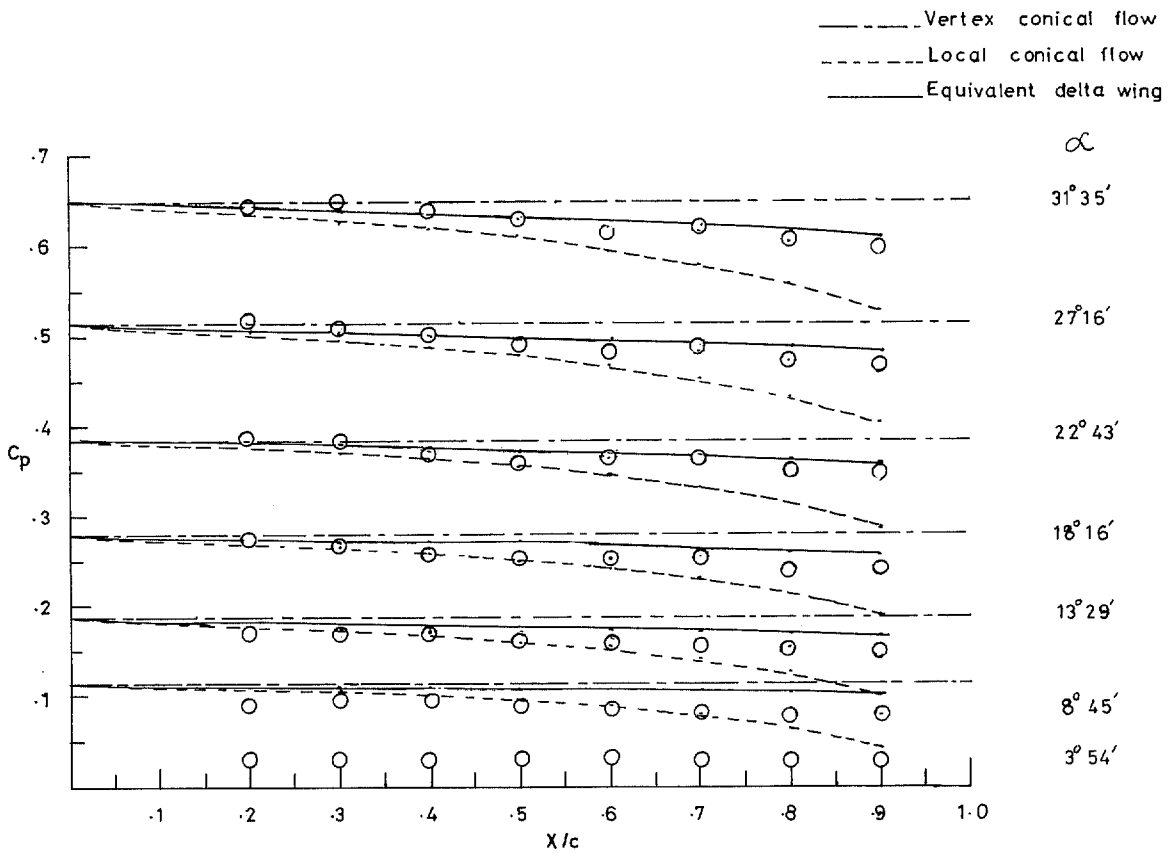


FIG. 2a. Centreline pressure distribution, Gothic wing, Mach number = 3.5.

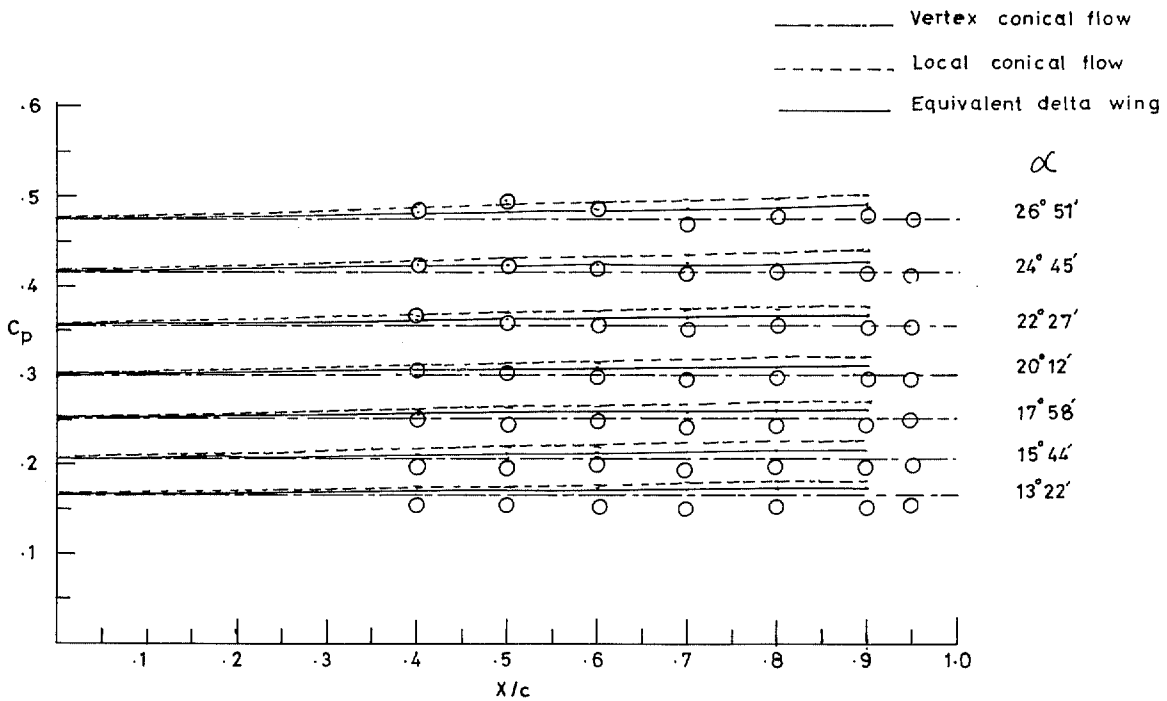


FIG. 2b. Centreline pressure distribution, Concave-leading-edge wing, Mach number = 3.5.

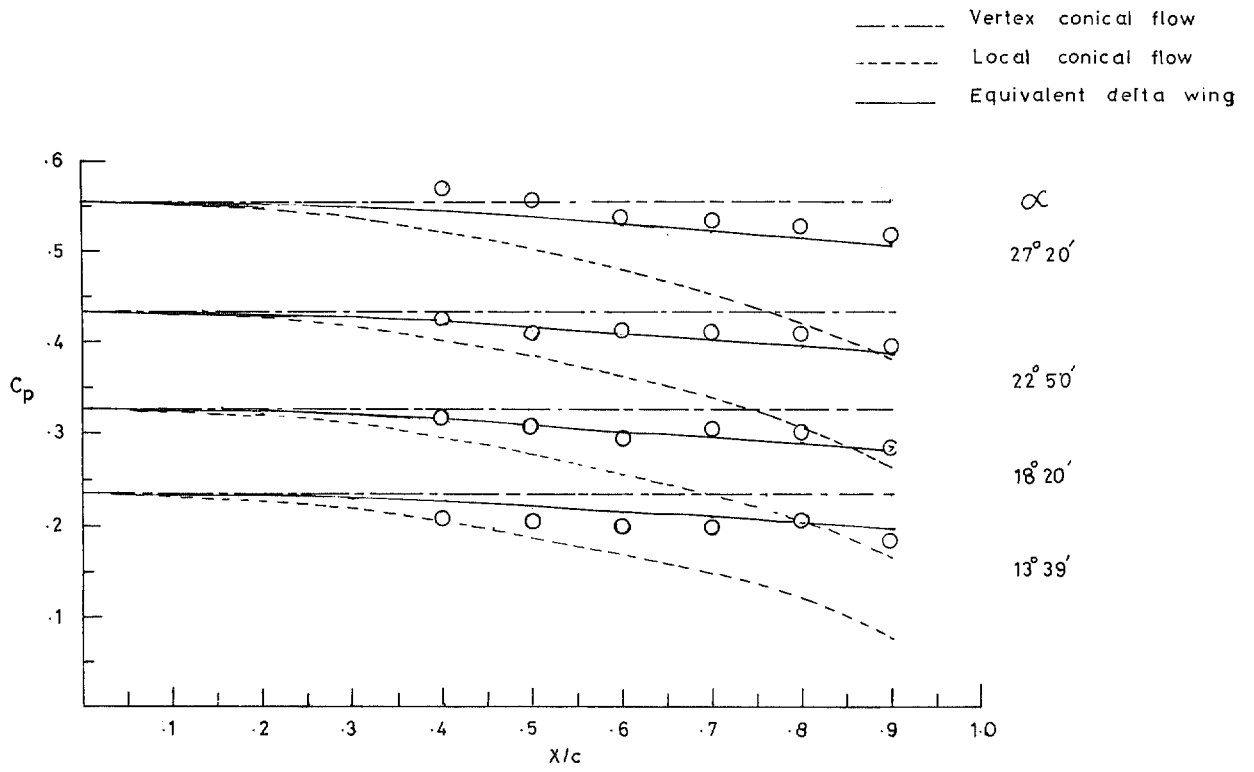


FIG. 2c. Centreline pressure distribution, Gothic wing, Mach number = 2.5.

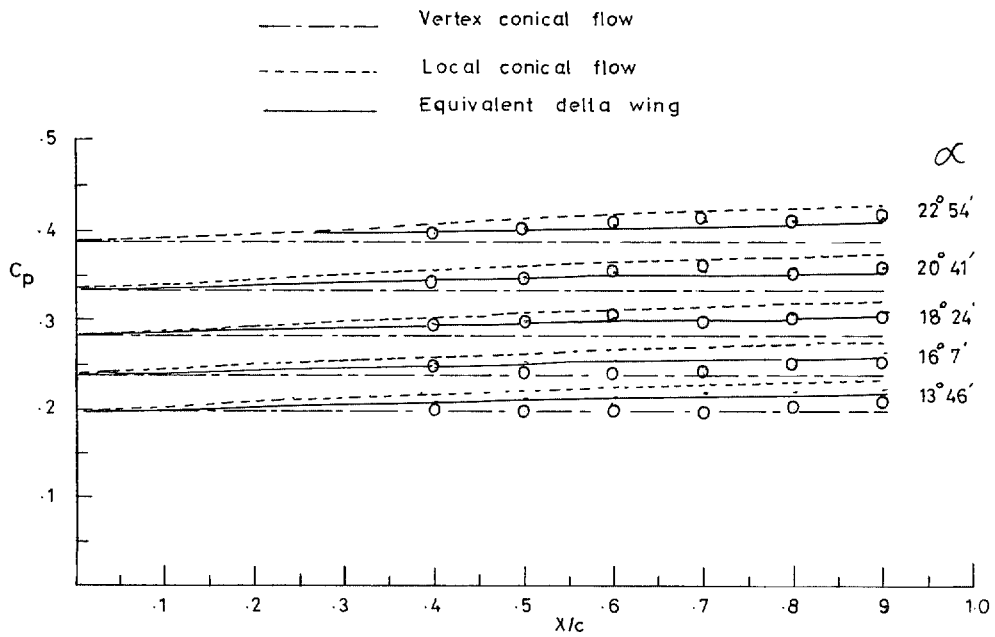


FIG. 2d. Centreline pressure distribution, Concave-leading-edge wing, Mach number = 2.5.

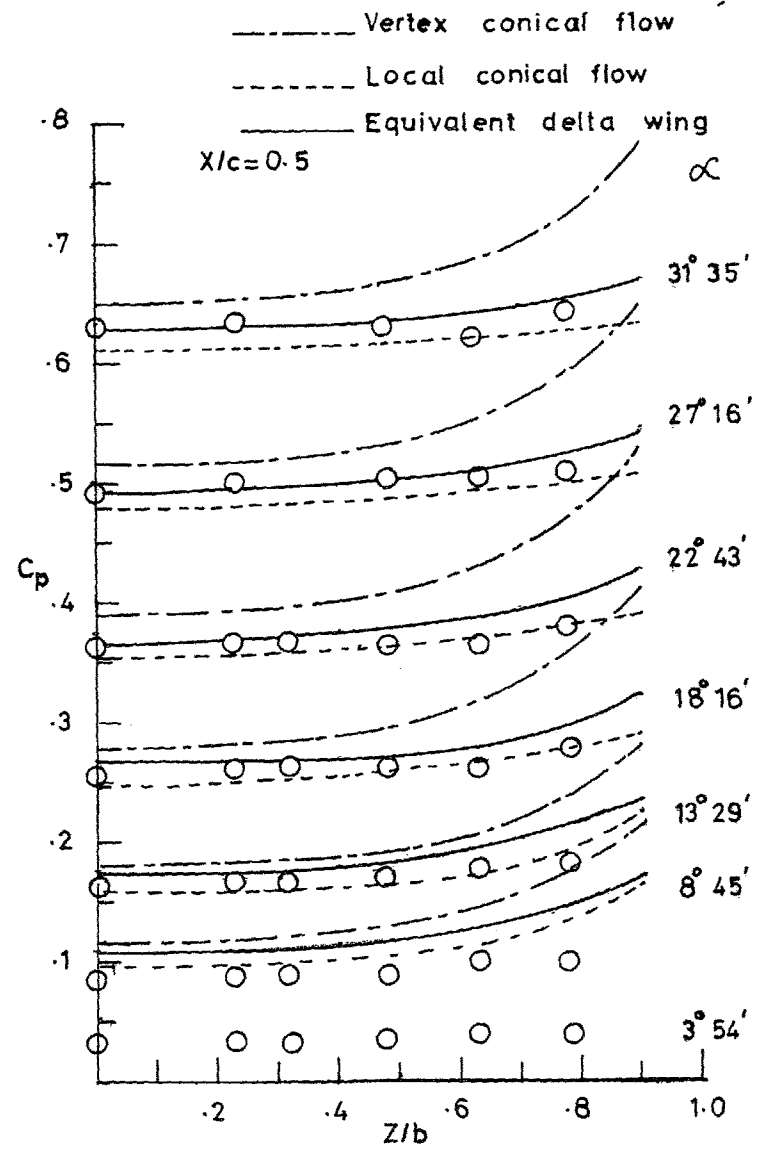
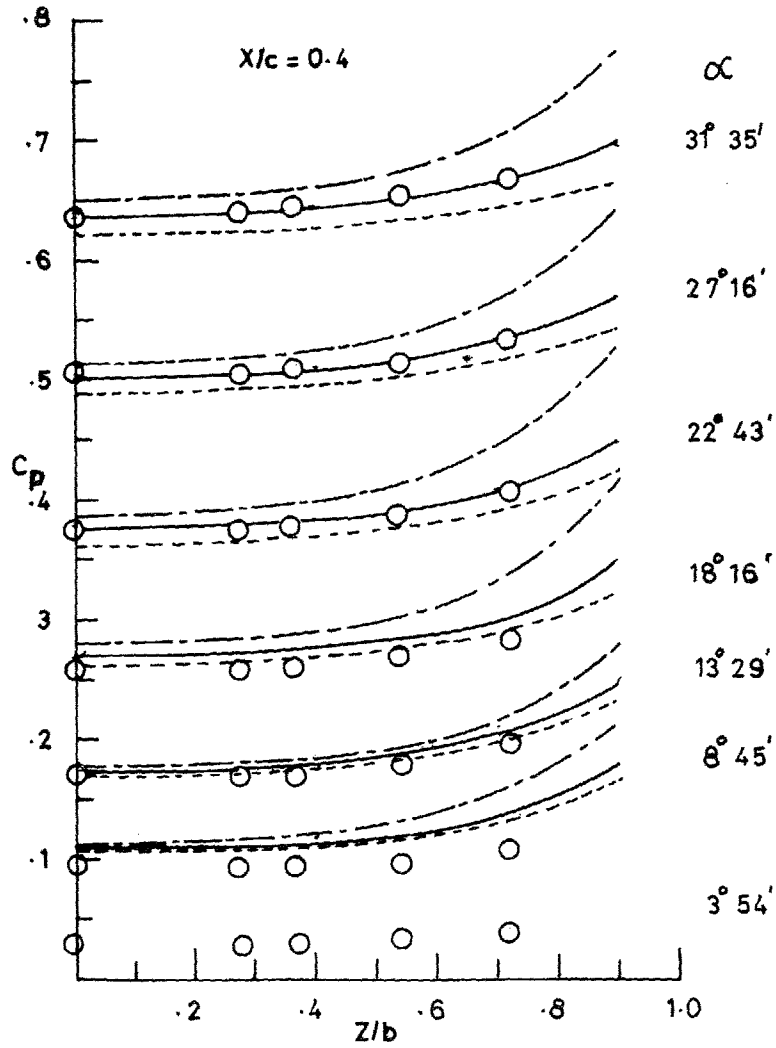


FIG. 3. Spanwise pressure distribution, Gothic wing, $M = 3.5$.

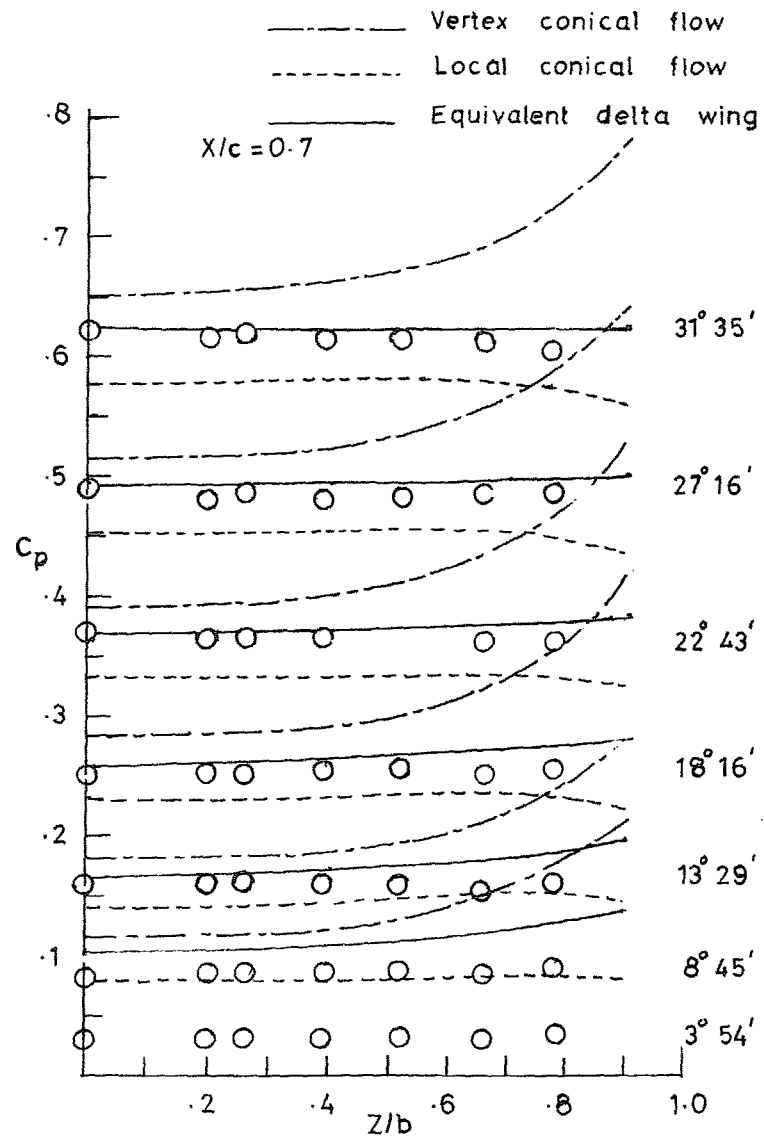
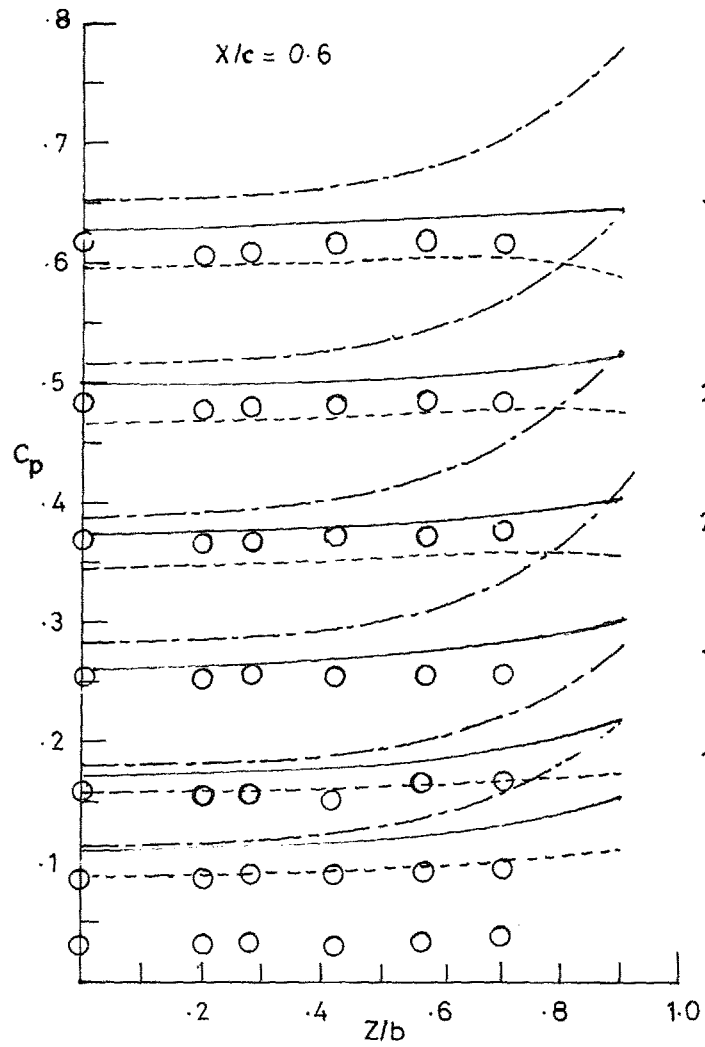


FIG. 3. Continued.

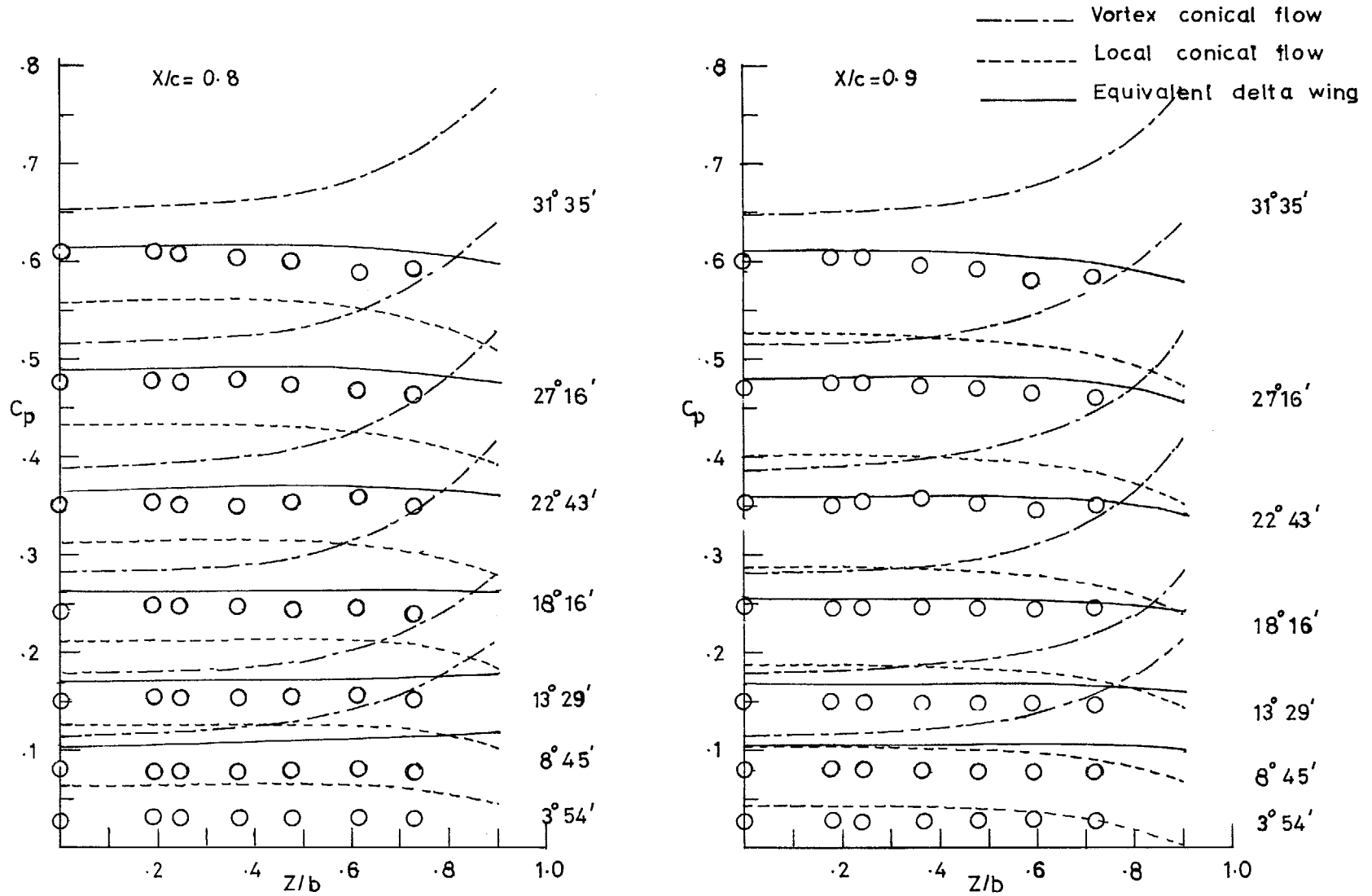


FIG. 3. Concluded.

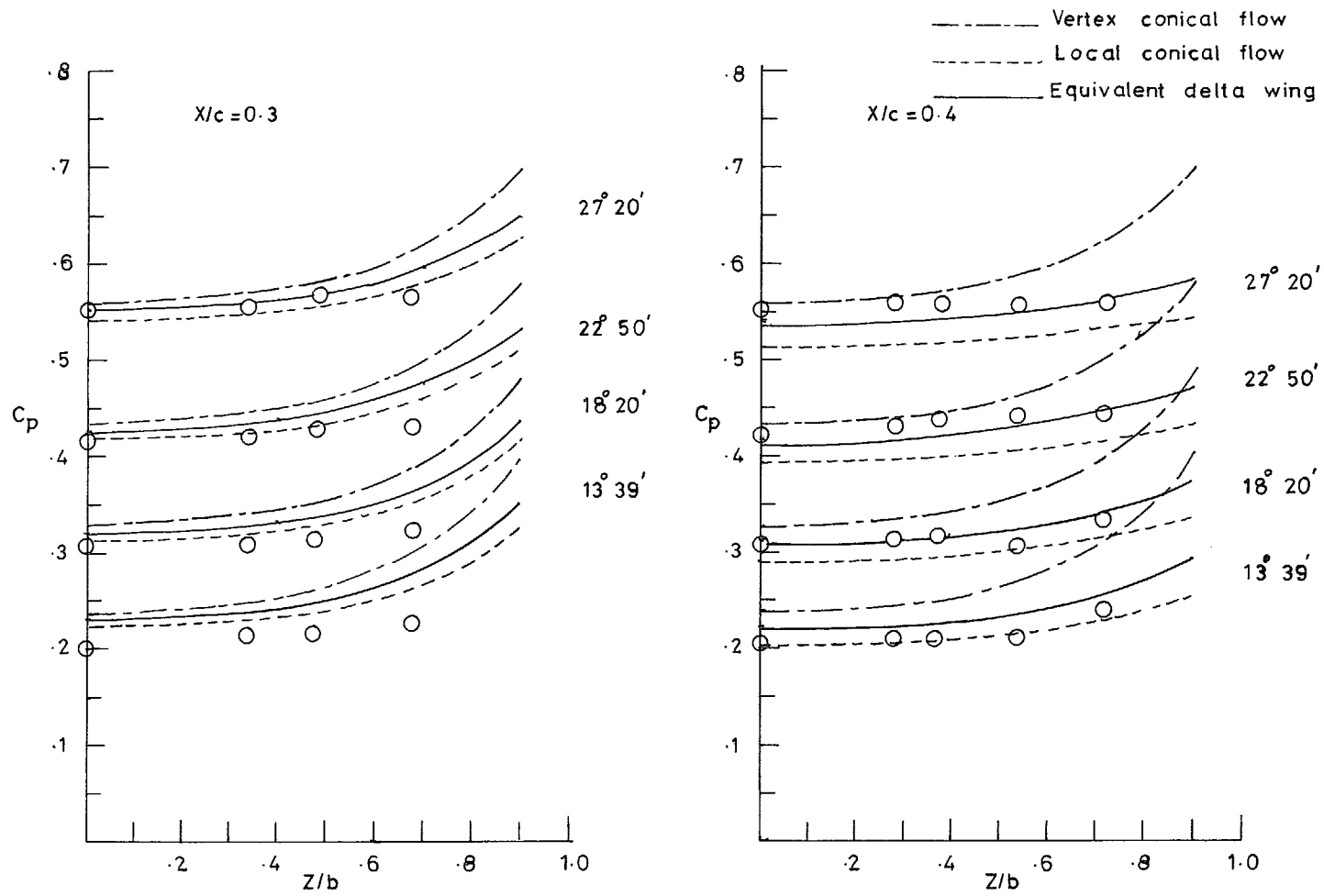


FIG. 4. Spanwise pressure distribution, Gothic wing, Mach number = 2.5.

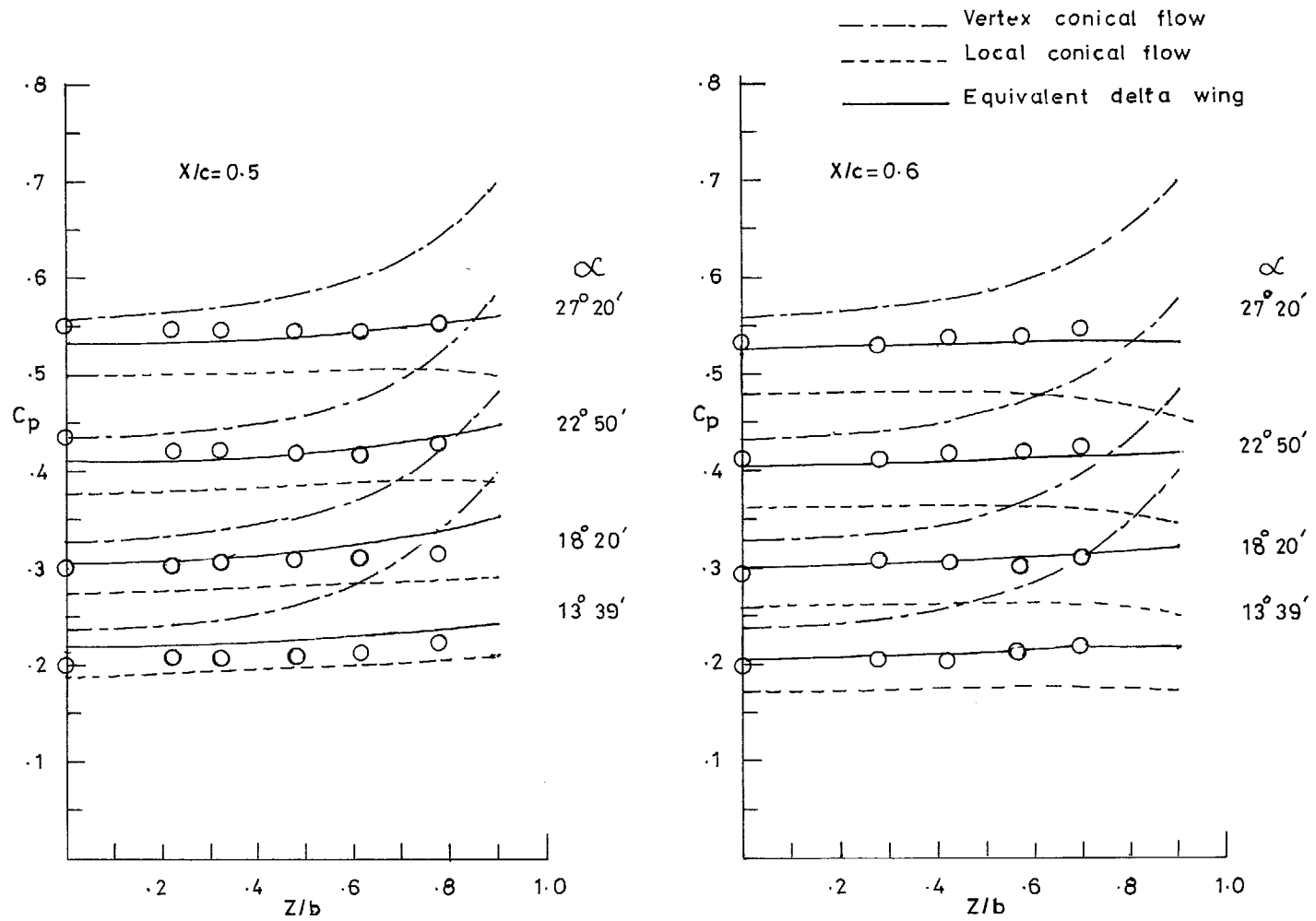


FIG. 4. Continued.

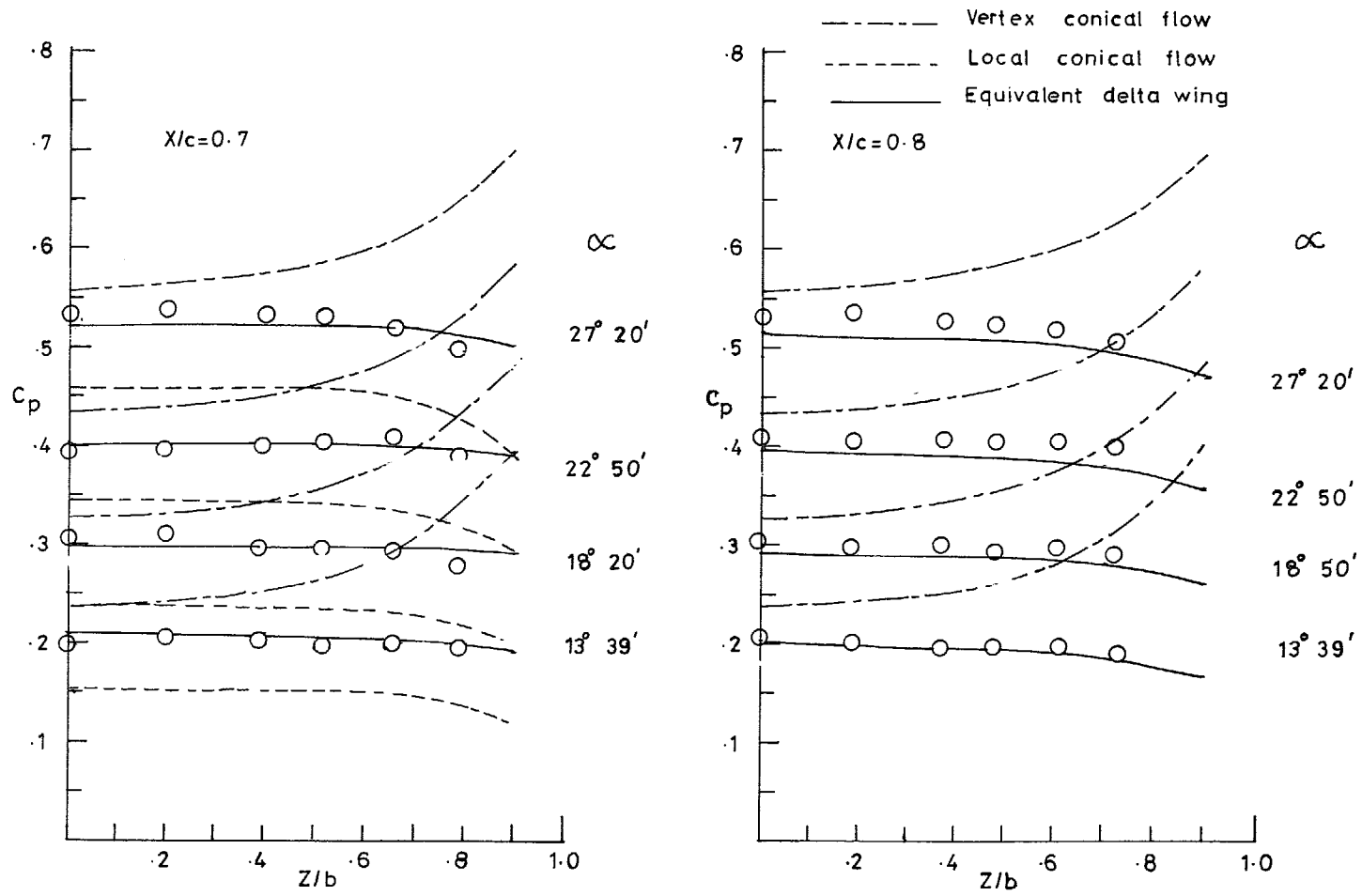


FIG. 4. Continued.

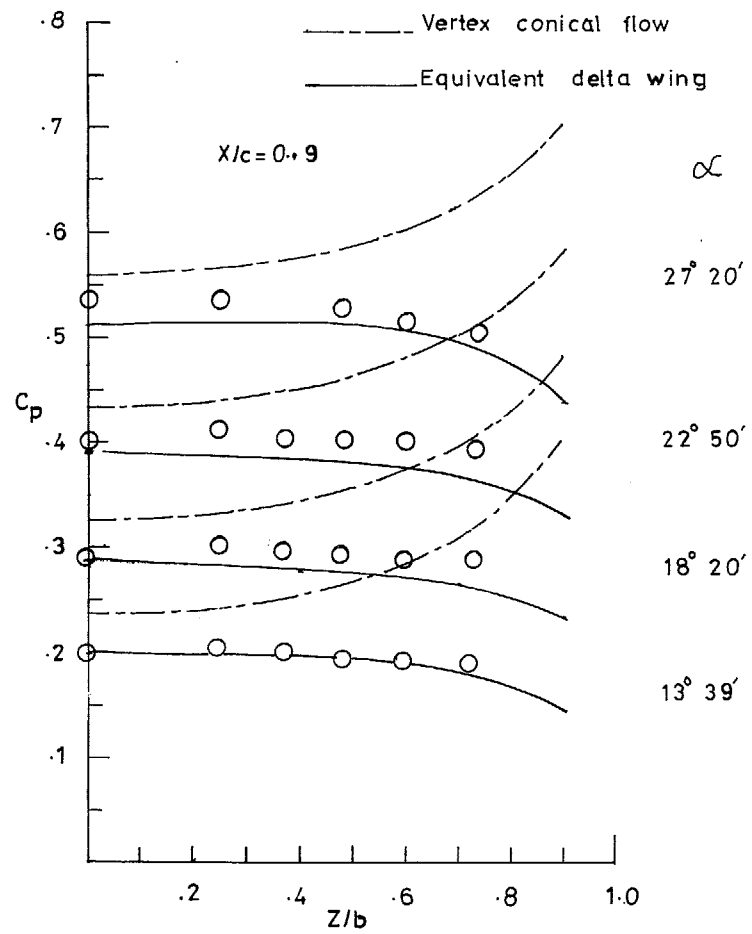
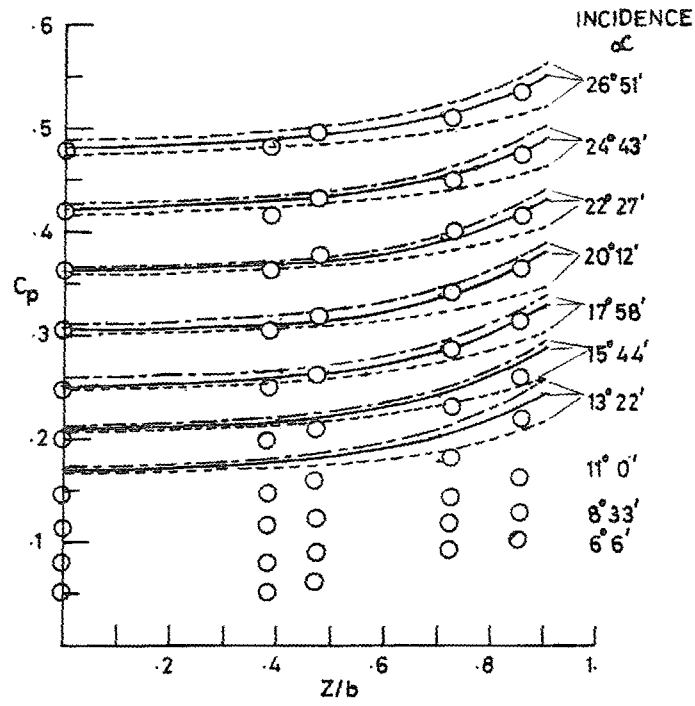


FIG. 4. Concluded.

----- Vertex conical flow
 - - - - - Local conical flow
 _____ Equivalent delta wing
 X/c = 0.4



X/c = 0.5

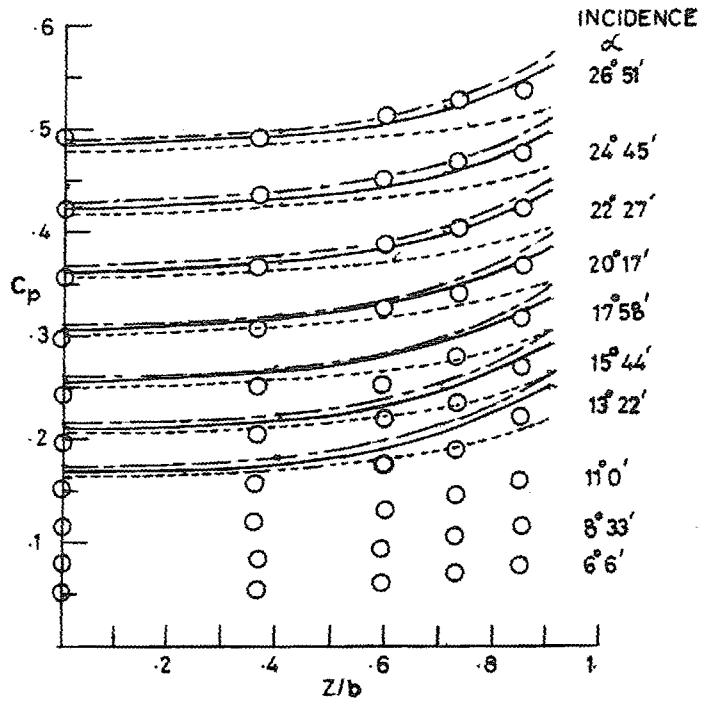


FIG. 5. Concave-leading-edge wing. Spanwise pressure distributions. Mach number = 3.5.

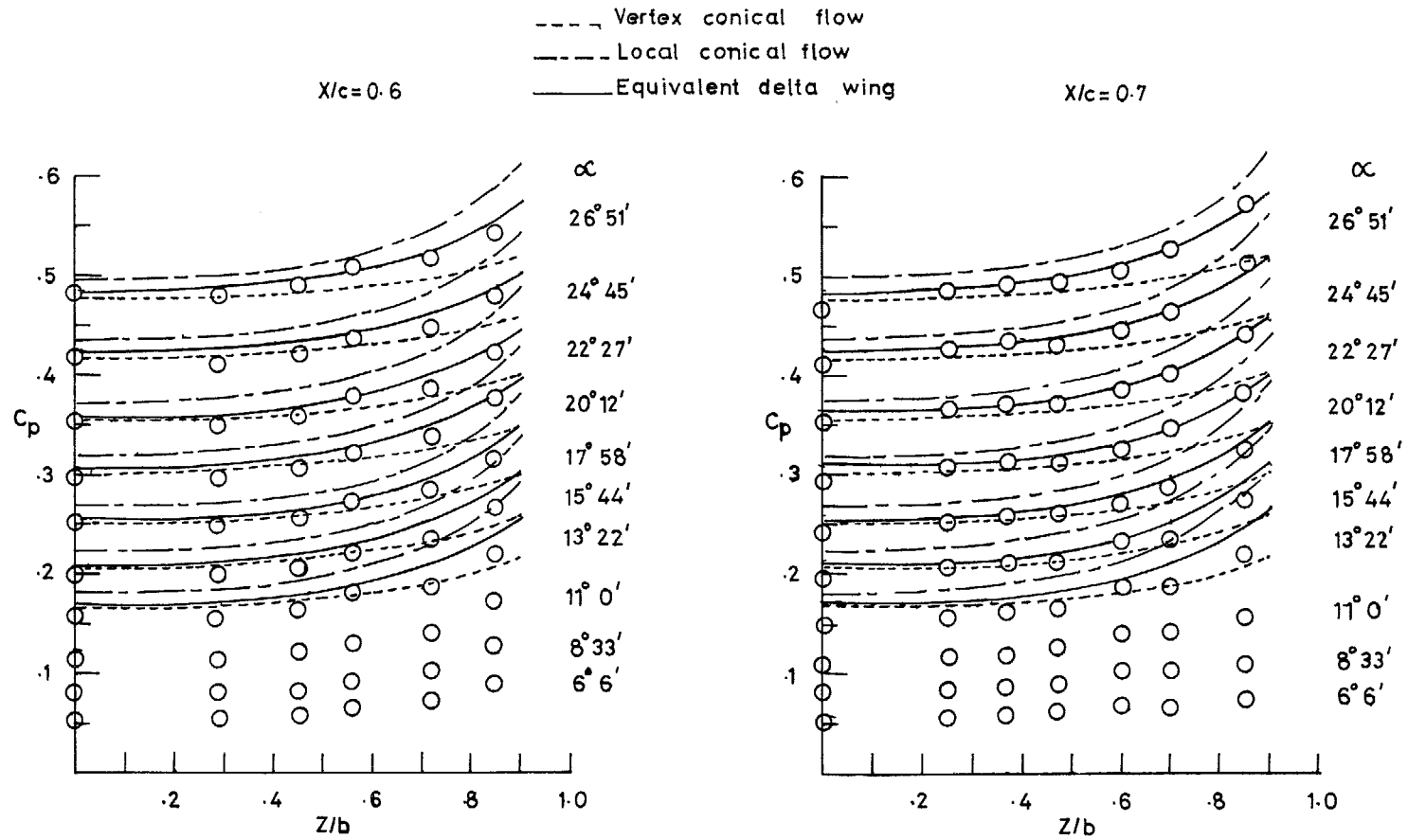


FIG. 5. Continued.

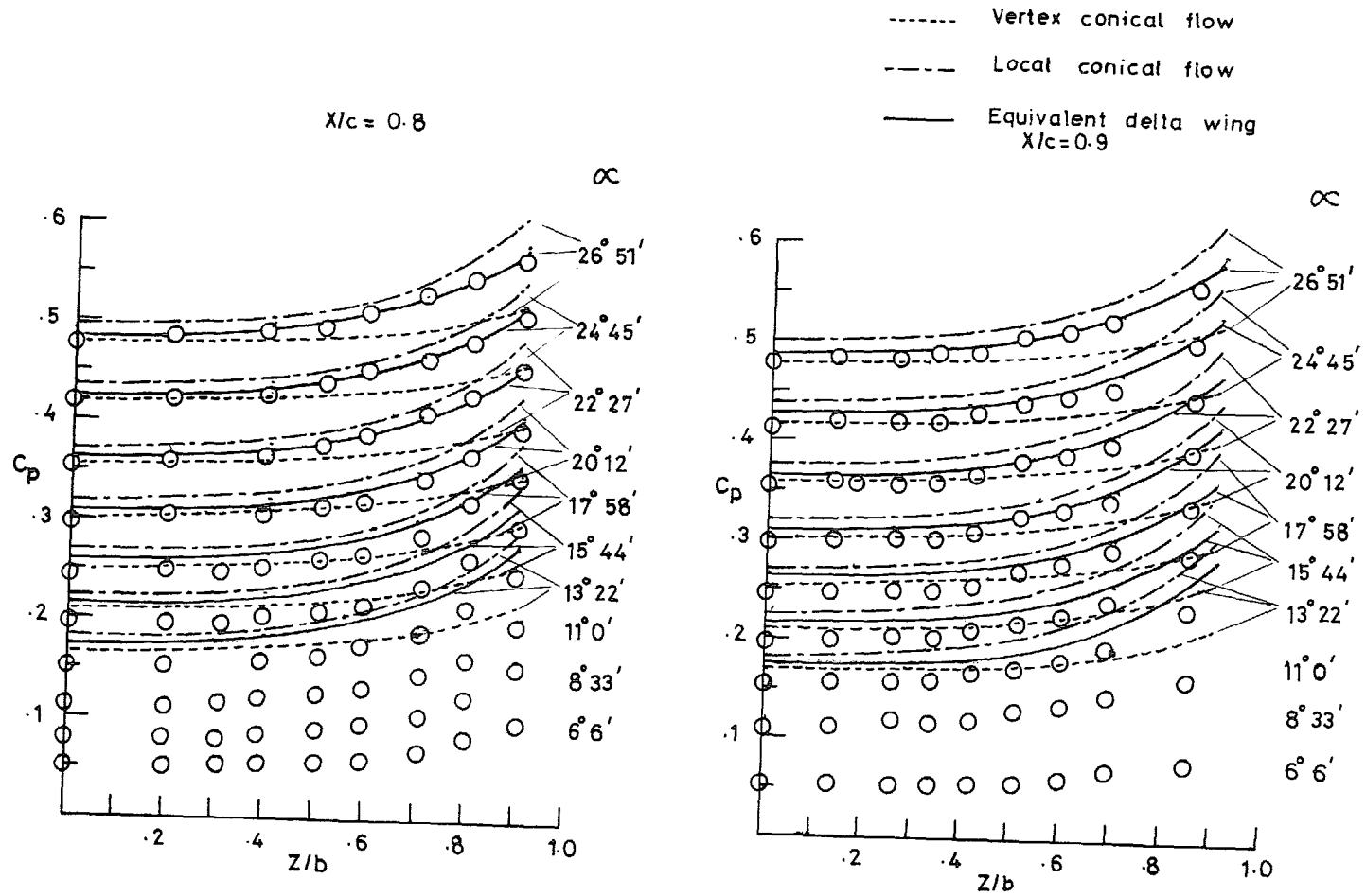


FIG. 5. Concluded.

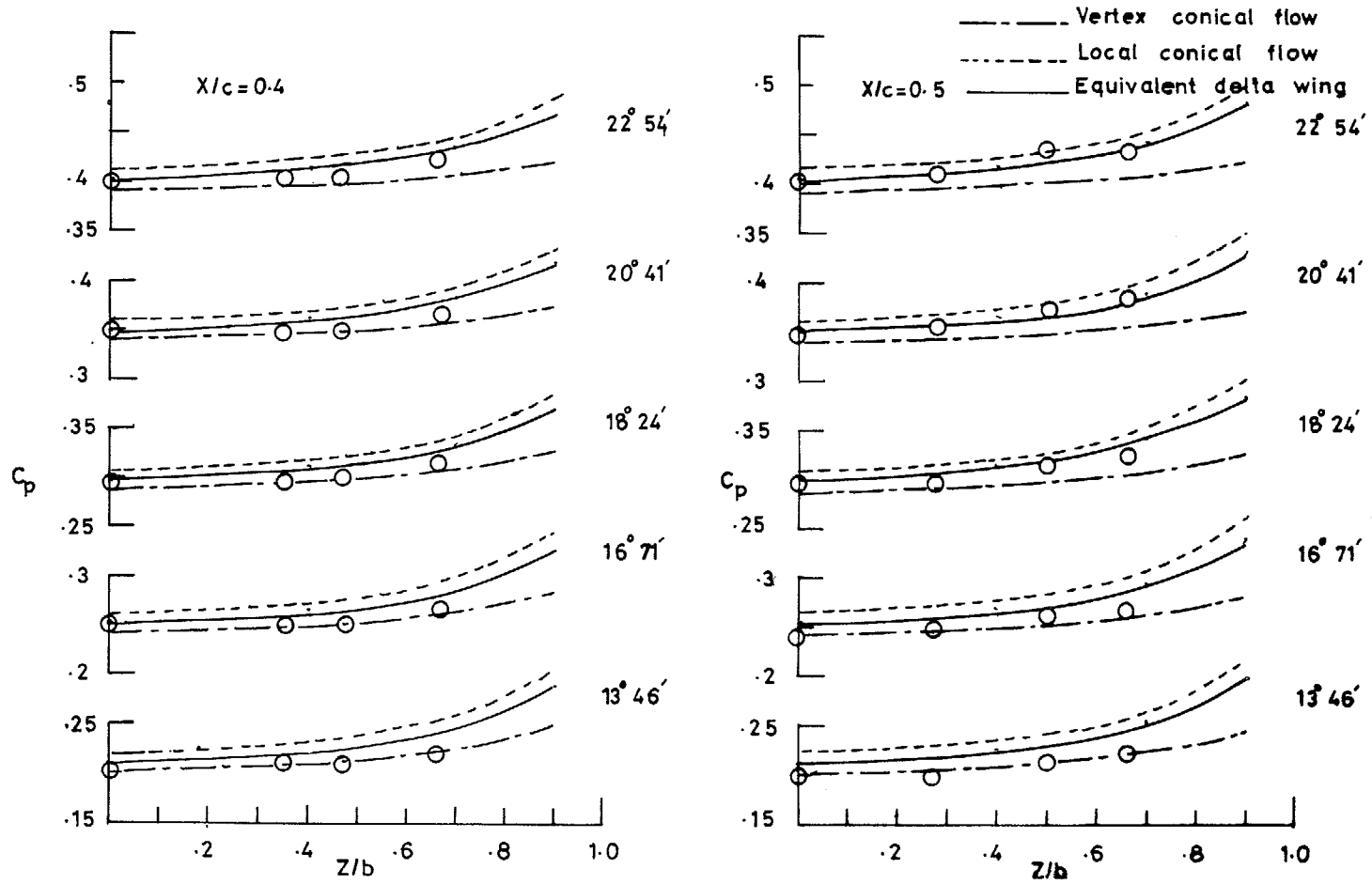


FIG. 6. Spanwise pressure distribution, Concave-leading-edge wing, Mach number = 2.5.

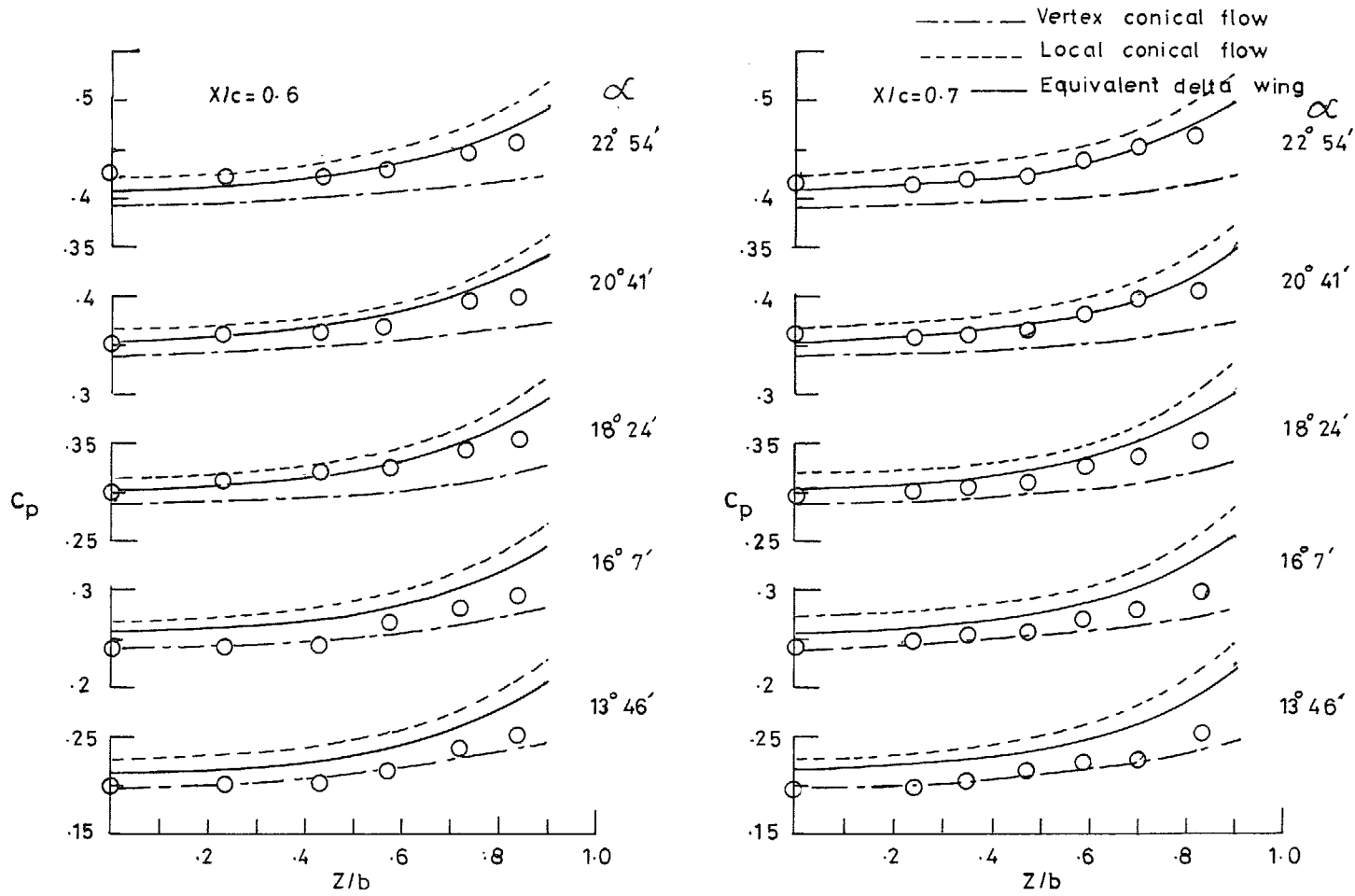


FIG. 6. Continued.

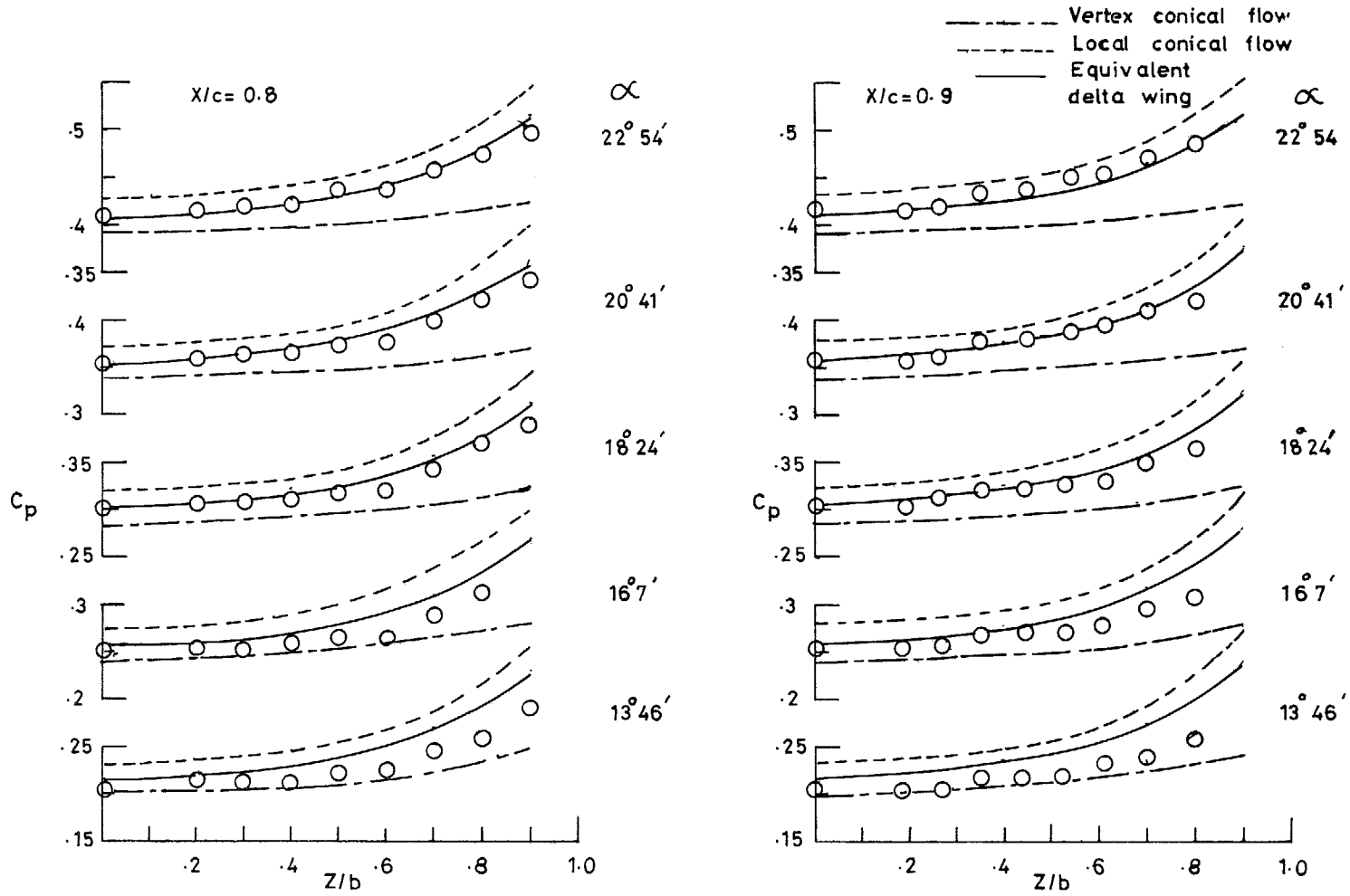


FIG. 6. Concluded.

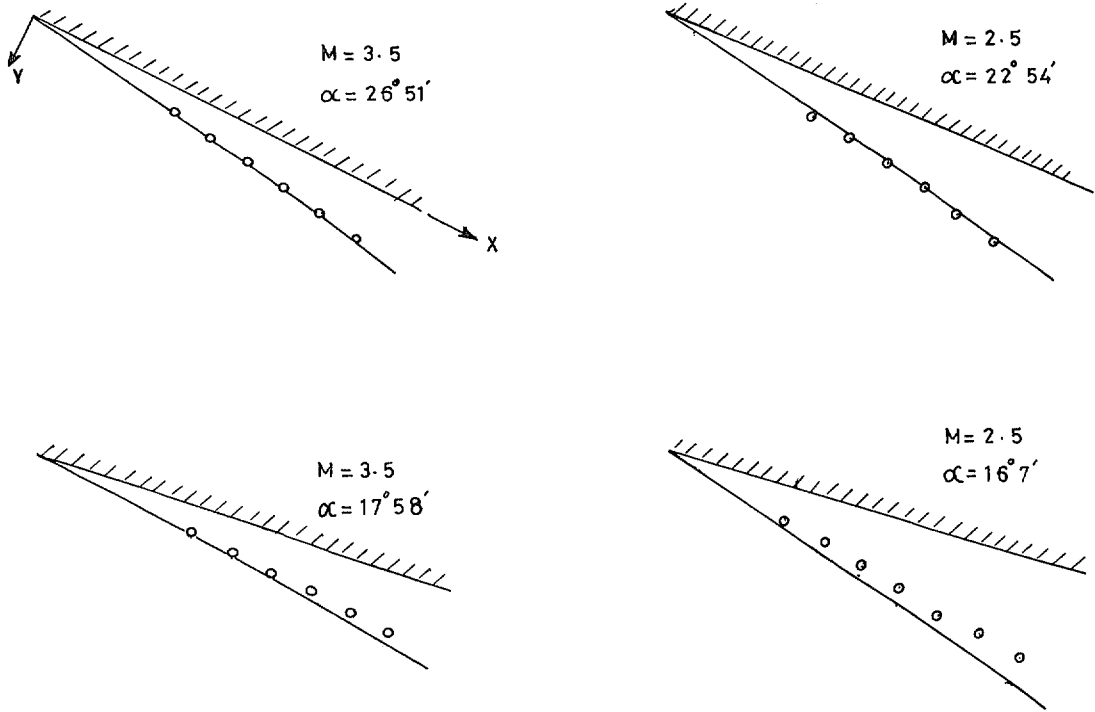


FIG. 7a. Centreline shock stand-off distance. Concave-leading-edge wing. — Estimation, \circ Measurement.

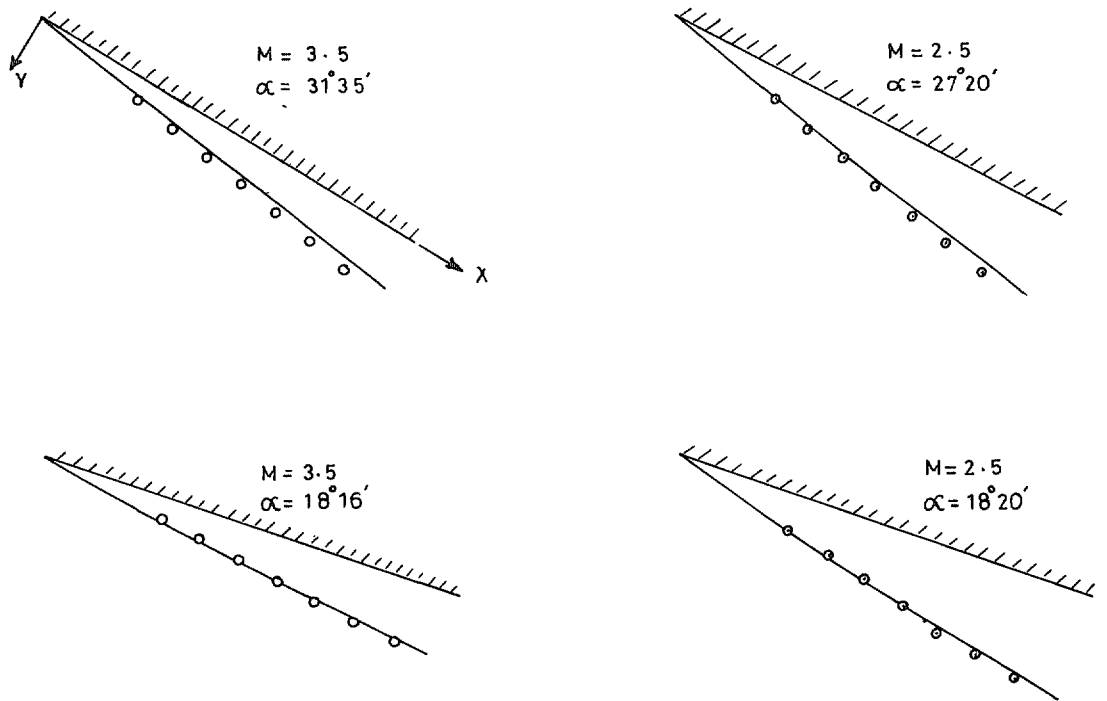


FIG. 7b. Centreline shock stand-off distance. Gothic wing. — Estimation, \circ Measurement.

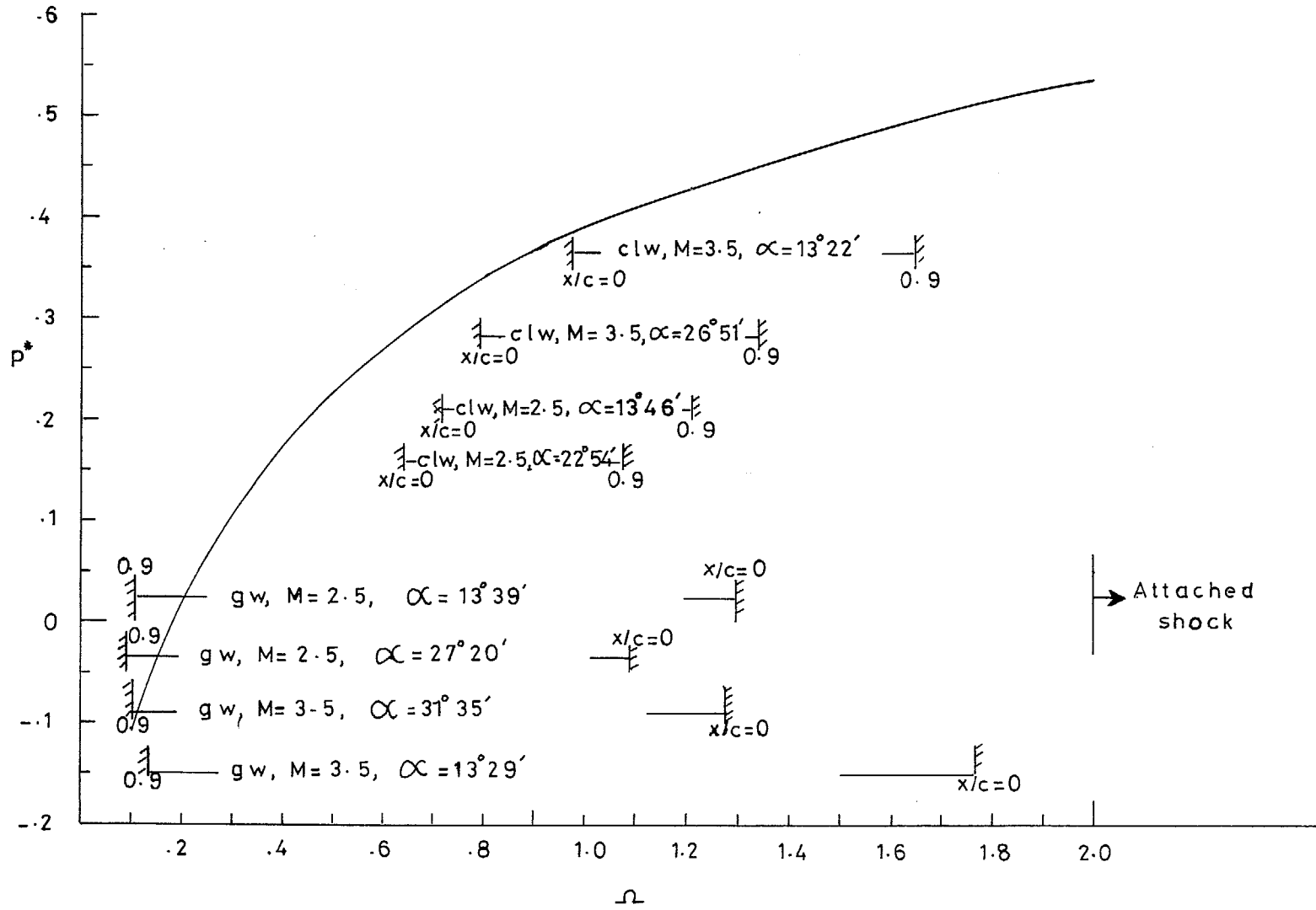


FIG. 8. $p^*(z/b = 0)$ versus Ω (gw = gothic wing, clw = concave-leading-edge wing).

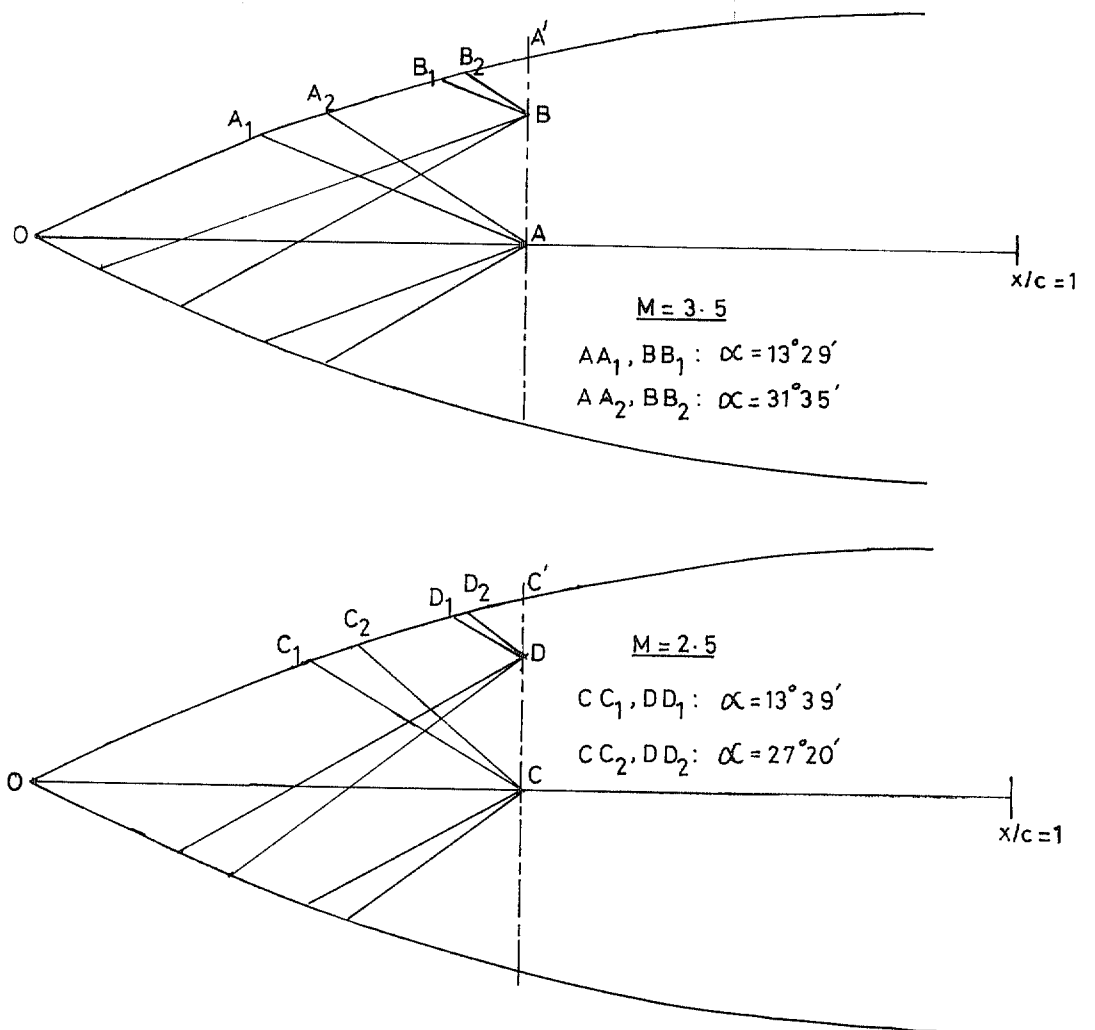


FIG. 9. Domains of dependence.

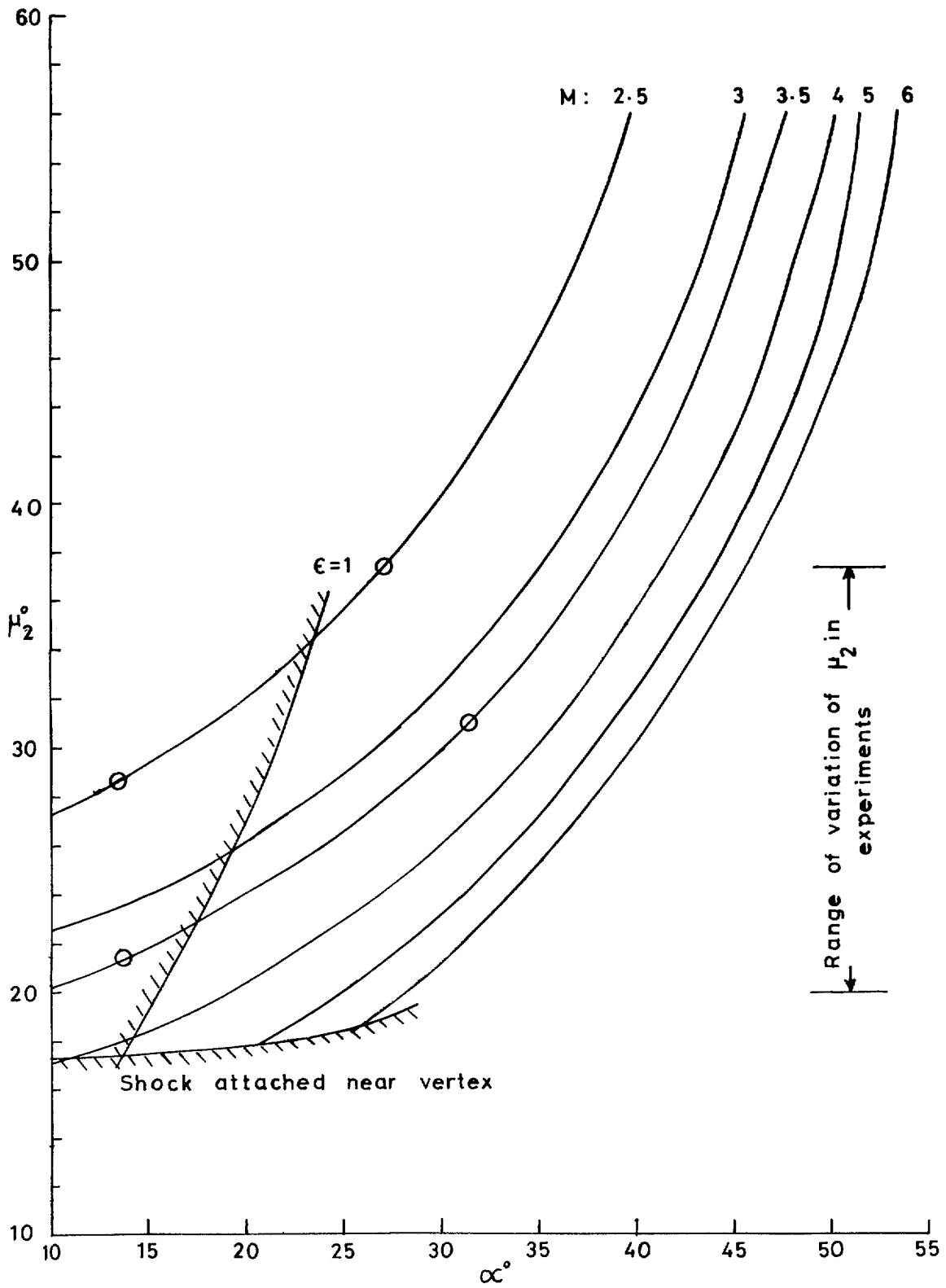
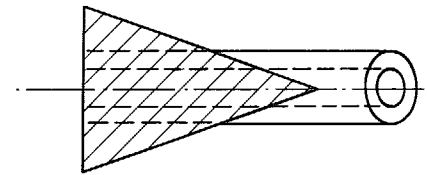
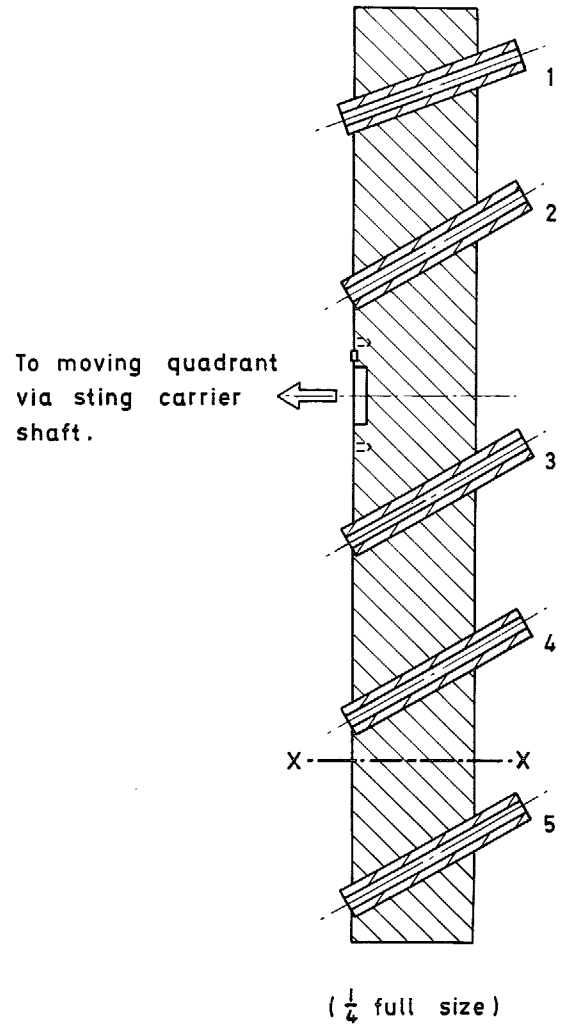


FIG. 10. Mach angle in the shock layer, Gothic wing, $x/c = 0.5$.



SECTION XX
($\frac{1}{2}$ full size)

Position 2 : Concave -leading -edge wing.
Position 3 : Gothic wing.

Model sting axes : all
except 1 are inclined
at 30° to horizontal.
1 inclined at 20° .

FIG. 11. Model carrier.

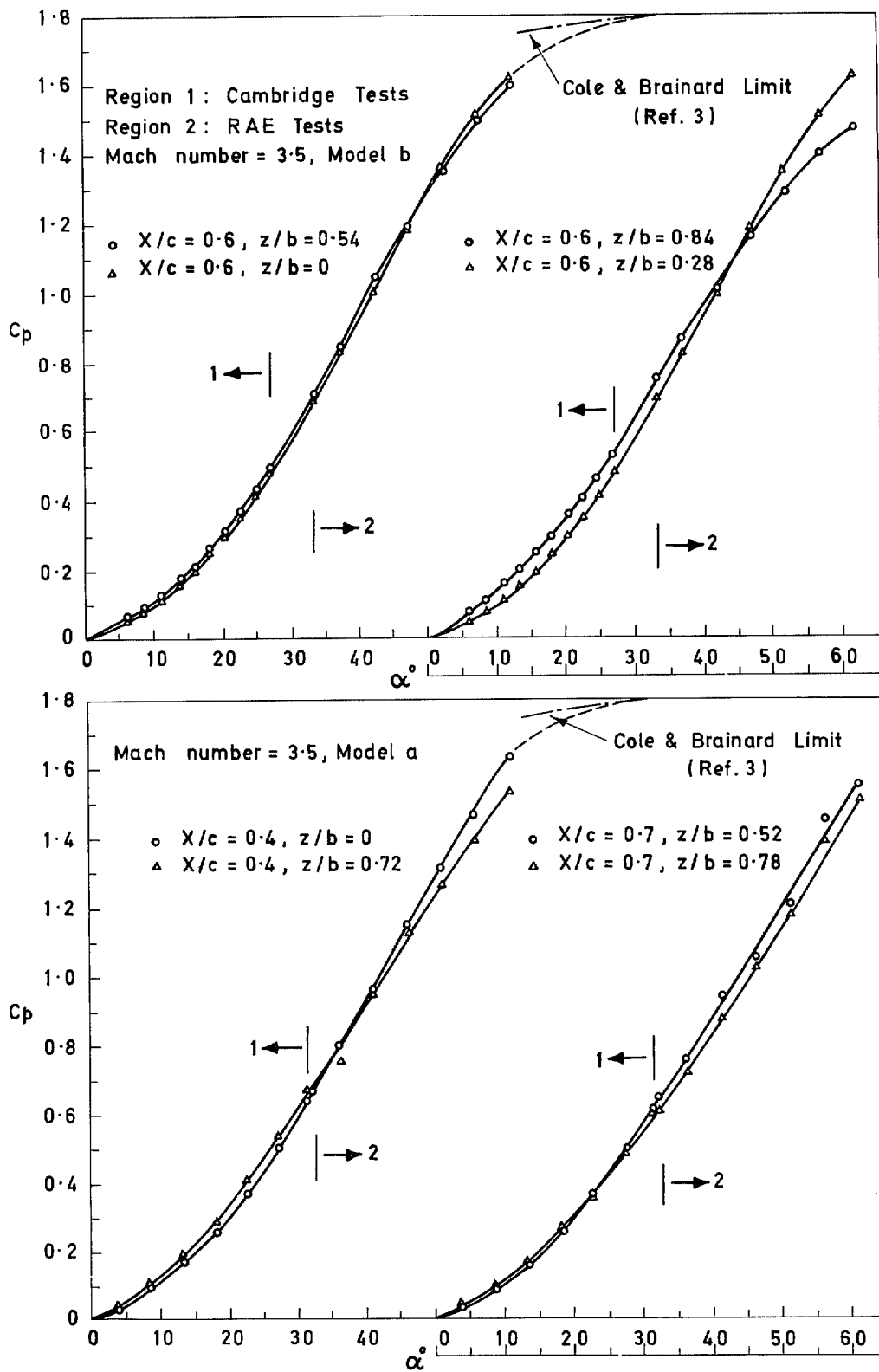


FIG. 12.

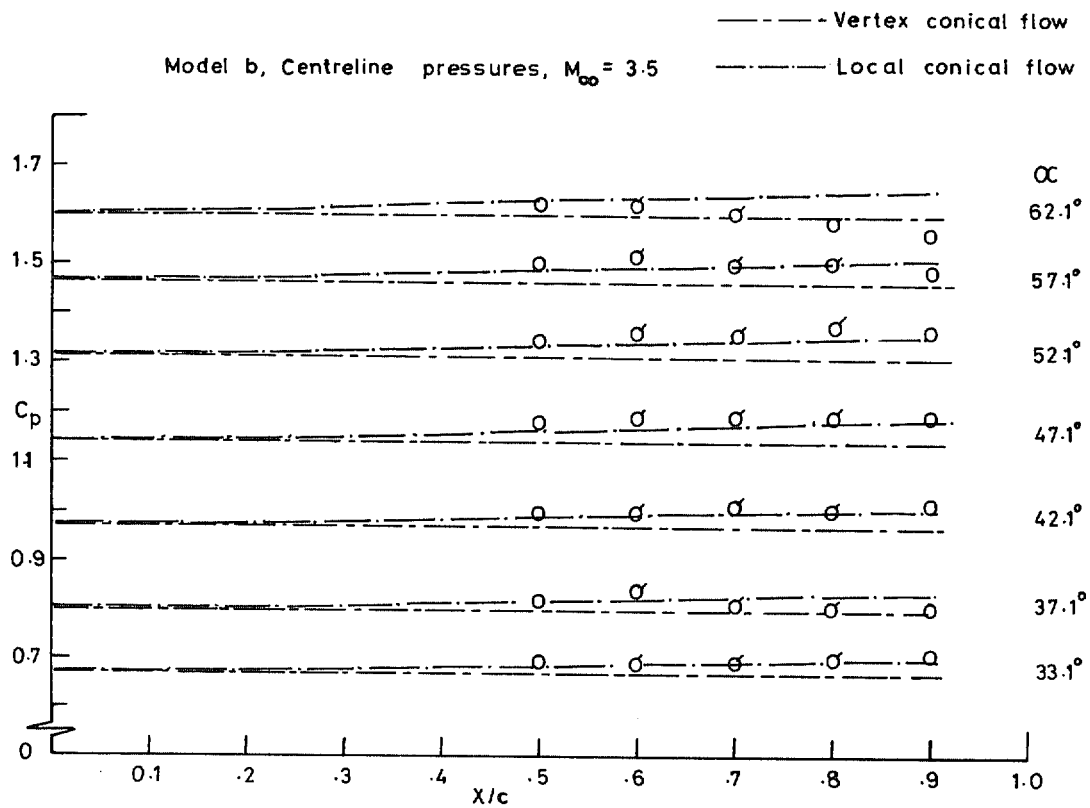


FIG. 13a.

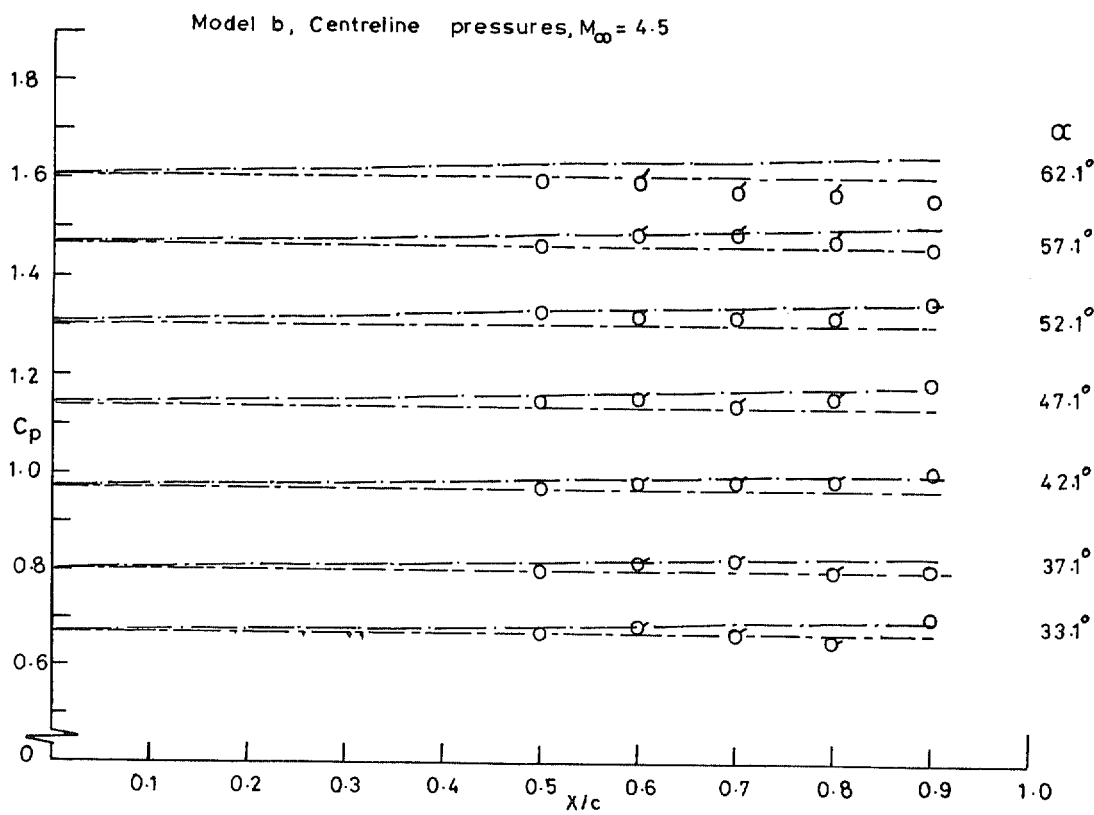


FIG. 13b.

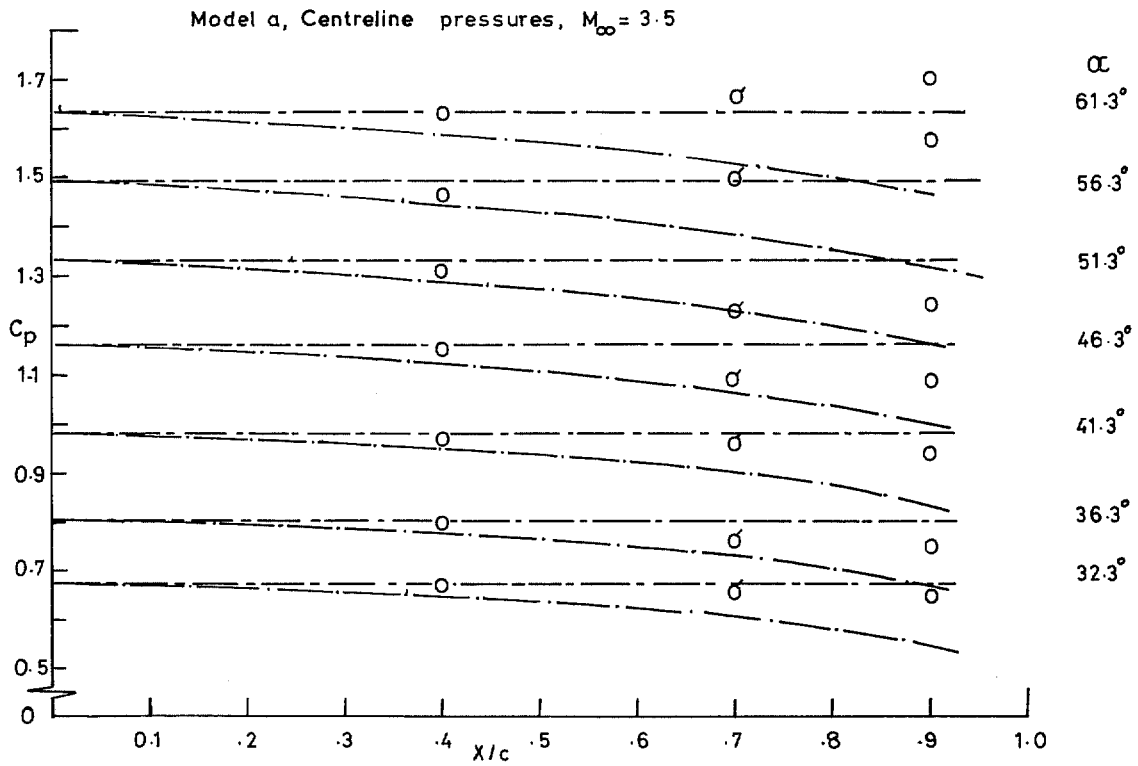


FIG. 13c.

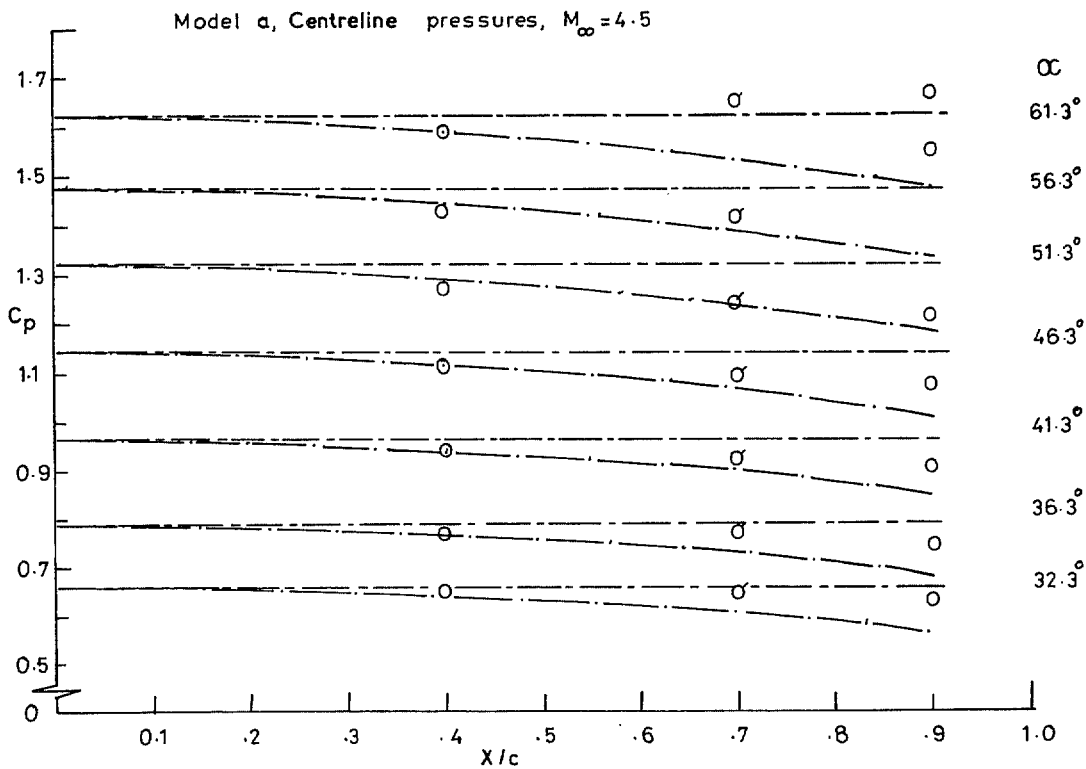


FIG. 13d.

Model b, Spanwise pressures, $M_\infty = 3.5$

38

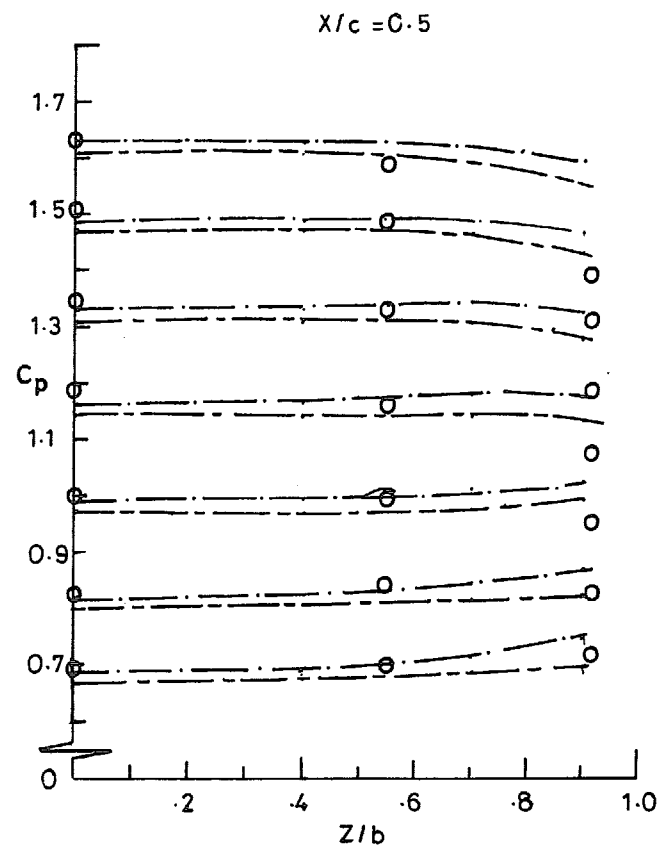
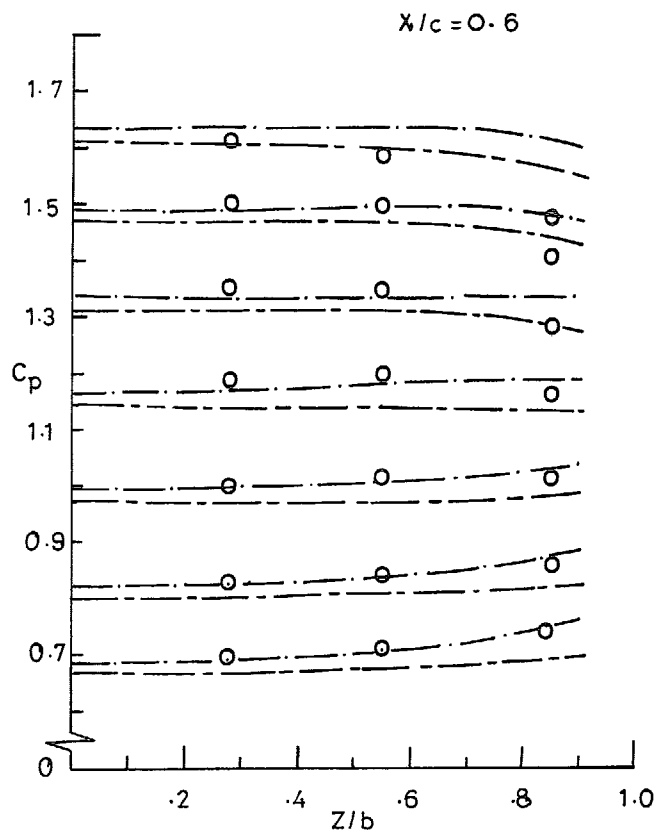


FIG. 14.

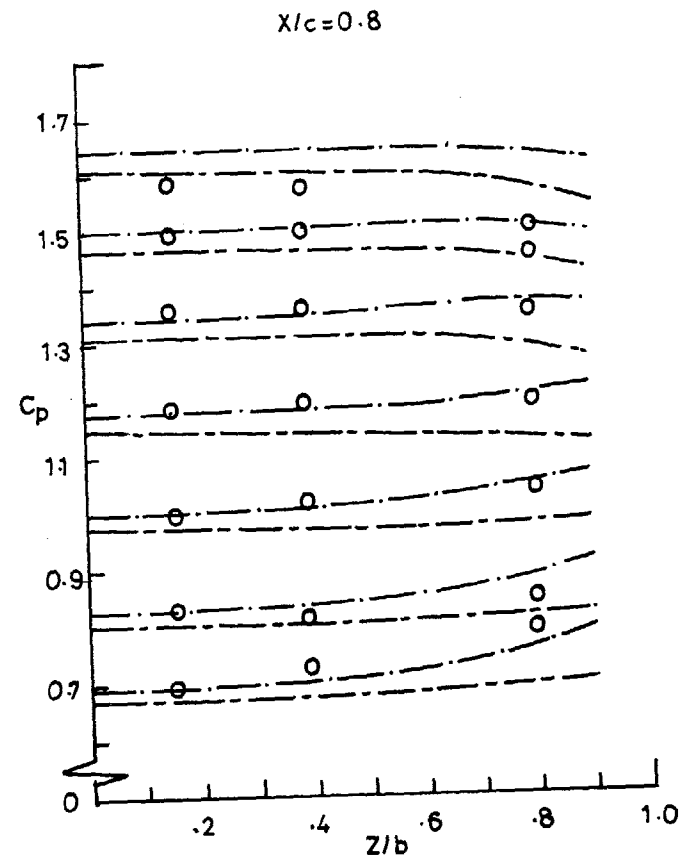
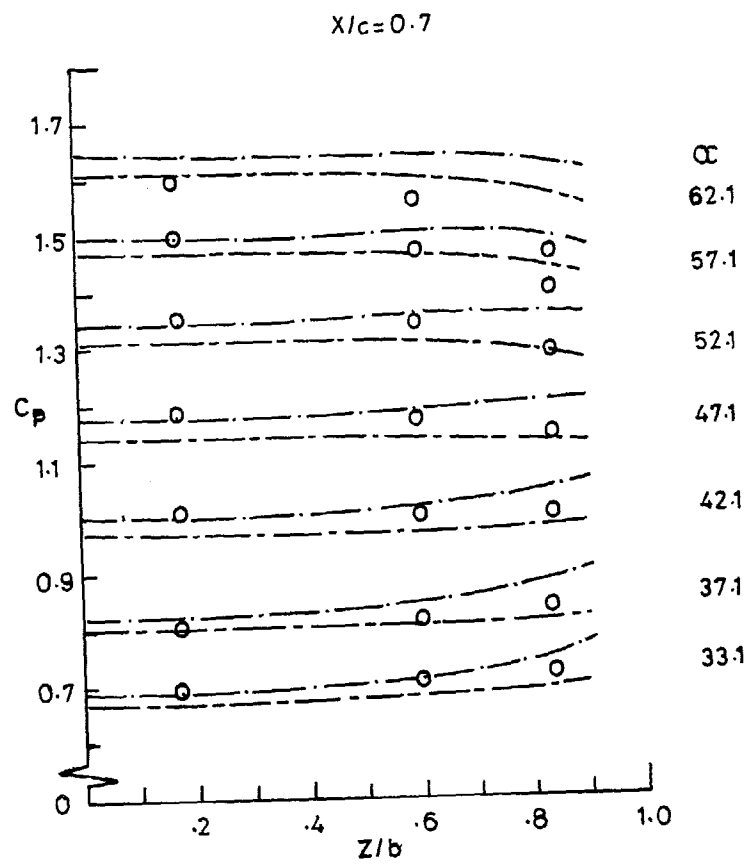


FIG. 14. Continued.

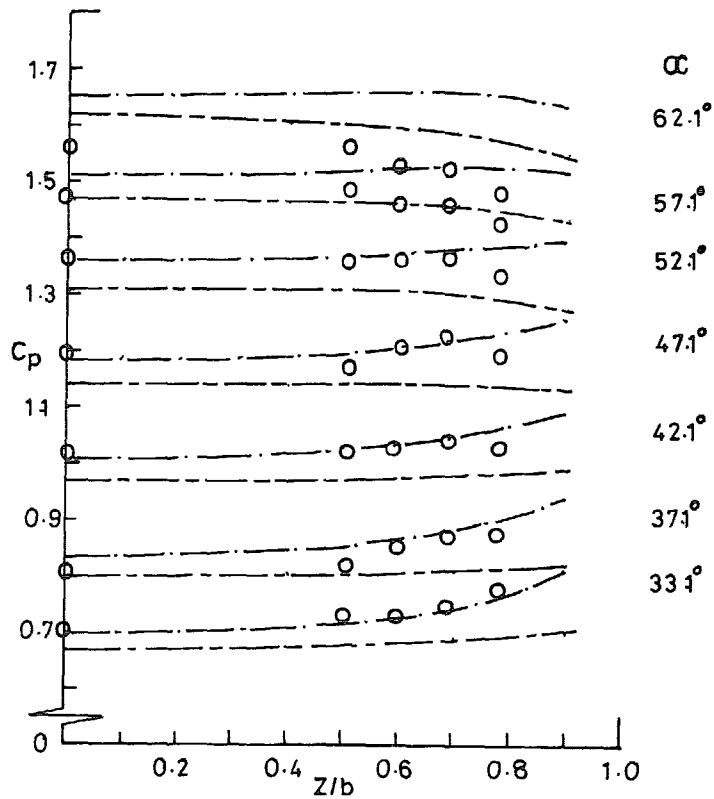


FIG. 14. Concluded.

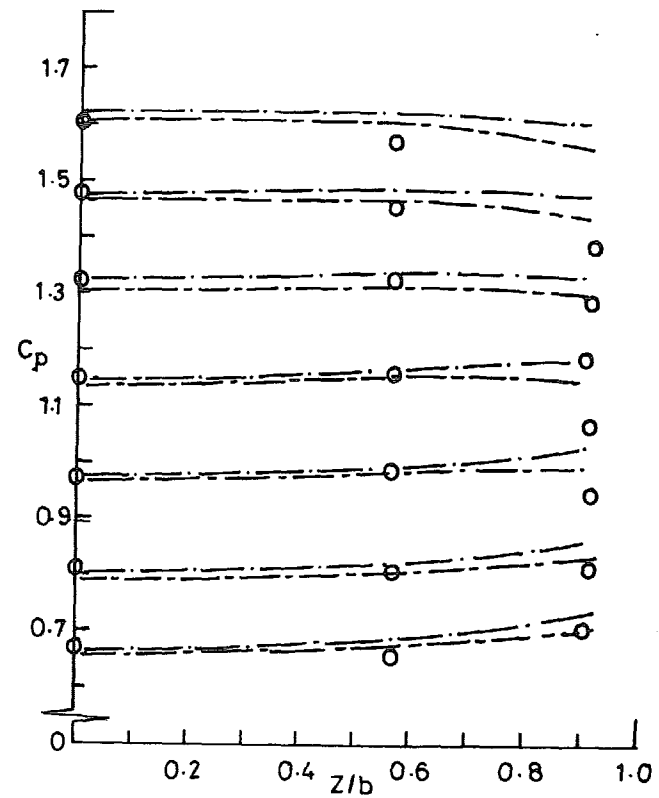
Model b, Spanwise pressures, $M=4.5$ 

FIG. 15.

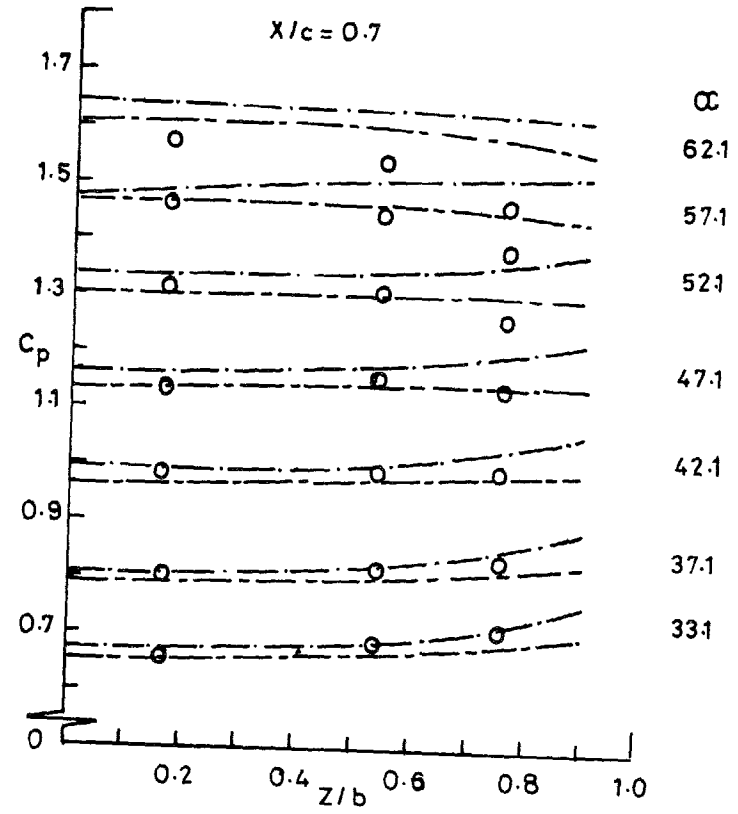
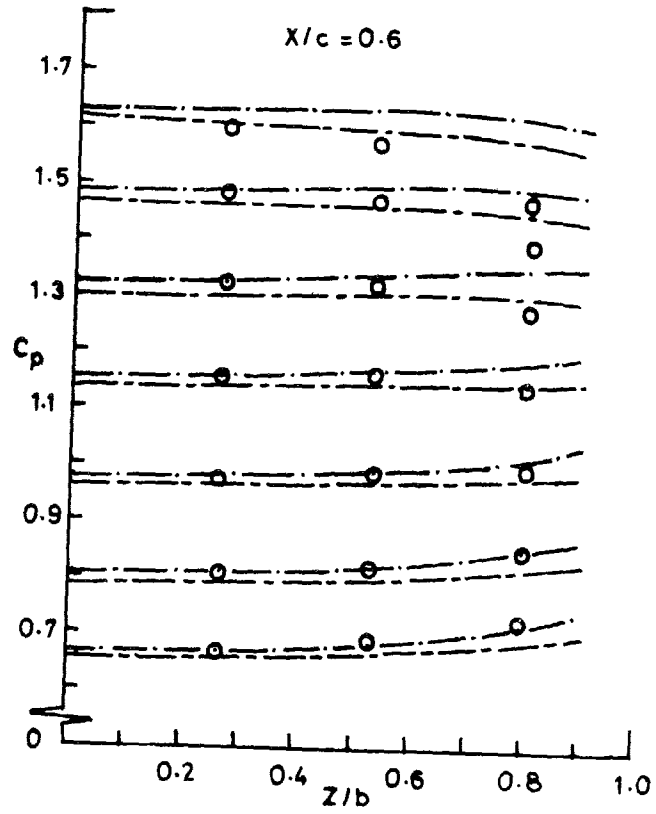


FIG. 15. Continued.

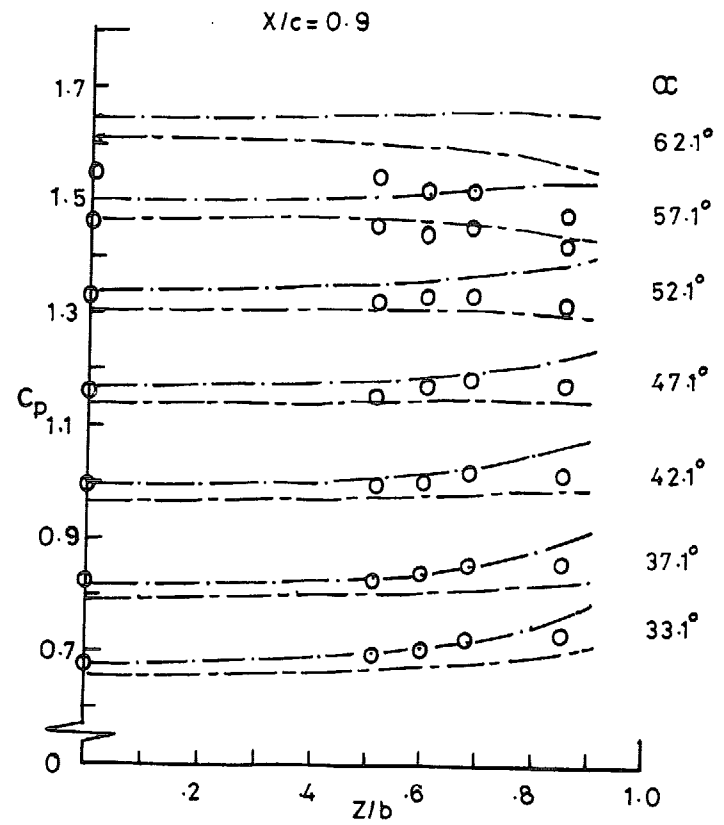
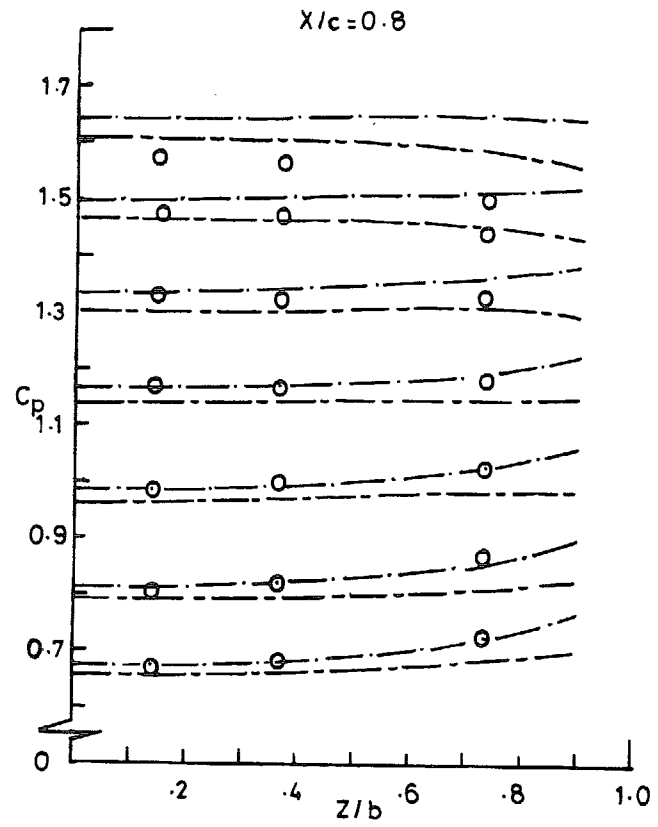


FIG. 15. Concluded.

Model a, Spanwise pressures, $M_\infty = 3.5$

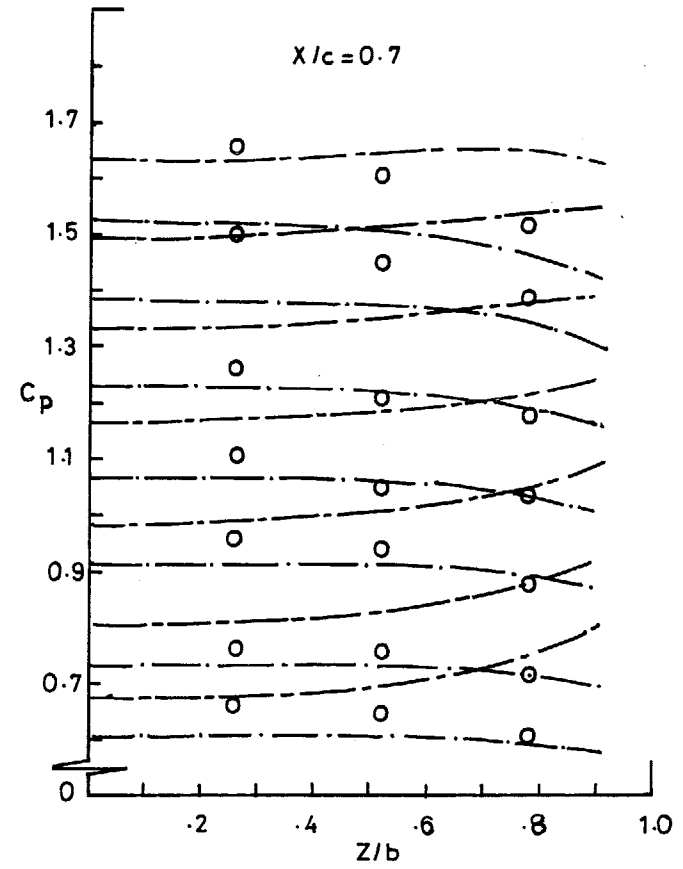
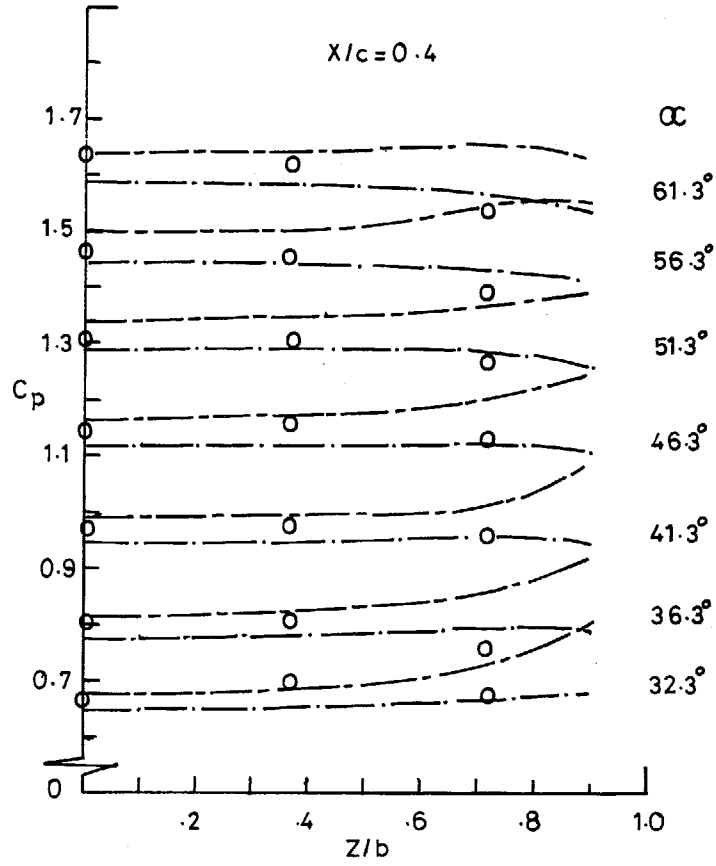


FIG. 16.

Model a, Spanwise pressures, $M_\infty = 4.5$

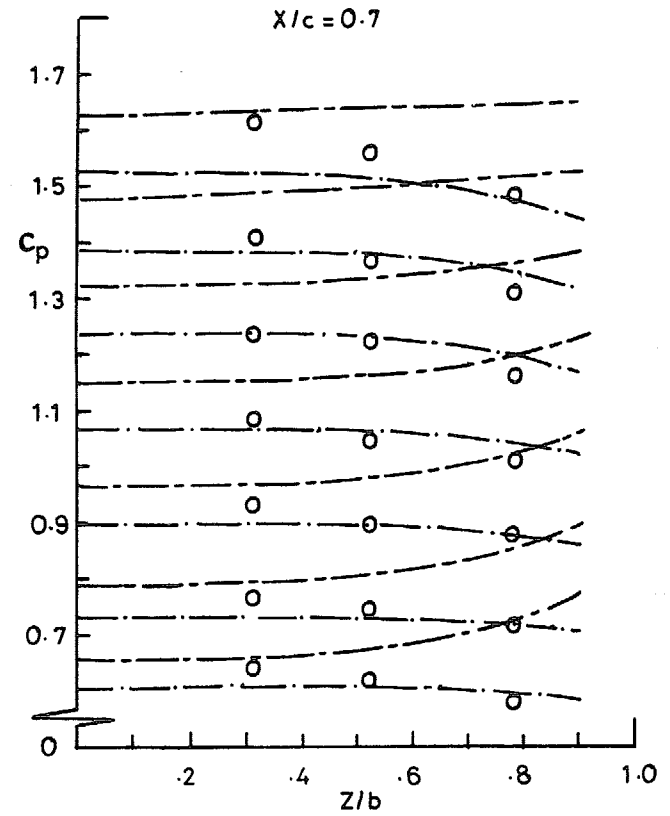
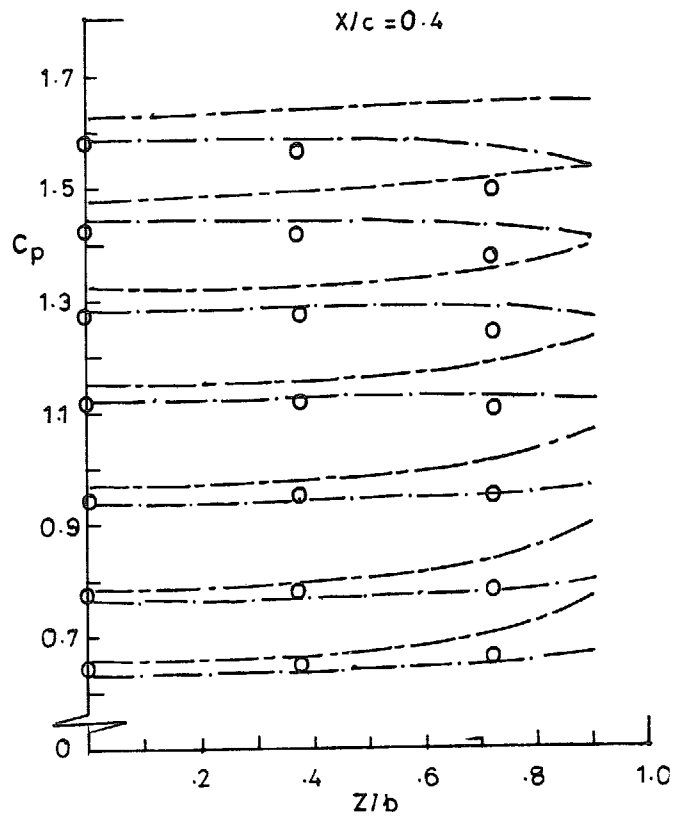


FIG. 17.

© Crown copyright 1974

HER MAJESTY'S STATIONERY OFFICE

Government Bookshops

49 High Holborn, London WC1V 6HB
13a Castle Street, Edinburgh EH2 3AR
41 The Hayes, Cardiff CF1 1JW
Brazenose Street, Manchester M60 8AS
Southey House, Wine Street, Bristol BS1 2BQ
258 Broad Street, Birmingham B1 2HE
80 Chichester Street, Belfast BT1 4JY

*Government publications are also available
through booksellers*